HHS Public Access

Author manuscript

Annu Rev Vis Sci. Author manuscript; available in PMC 2020 February 05.

Published in final edited form as:

Annu Rev Vis Sci. 2019 September 15; 5: 15–45. doi:10.1146/annurev-vision-091517-034239.

Imaging Retinal Activity in the Living Eye

Jennifer J. Hunter[1,2], **William H. Merigan**[1], **Jesse B. Schallek**[1,3]

[1]Flaum Eye Institute, Center for Visual Science, University of Rochester, Rochester, New York 14604, USA;

[2]The Institute of Optics, Department of Biomedical Engineering, University of Rochester, Rochester, New York 14604, USA

[3]Department of Neuroscience, University of Rochester, Rochester, New York 14604, USA

Abstract

Retinal function has long been studied with psychophysical methods in humans, whereas detailed functional studies of vision have been conducted mostly in animals owing to the invasive nature of physiological approaches. There are exceptions to this generalization, for example, the electroretinogram. This review examines exciting recent advances using in vivo retinal imaging to understand the function of retinal neurons. In some cases, the methods have existed for years and are still being optimized. In others, new methods such as optophysiology are revealing novel patterns of retinal function in animal models that have the potential to change our understanding of the functional capacity of the retina. Together, the advances in retinal imaging mark an important milestone that shifts attention away from anatomy alone and begins to probe function of healthy and diseased eyes.

Keywords

functional imaging; intrinsic signals; calcium indicator; optical coherence tomography; neurovascular coupling; adaptive optics

1. INTRODUCTION

Vision is initiated with the activity of multiple classes of cells that detect and process light in the retina. Although decades of research have contributed to an understanding of the molecular and electrical events in retinal neurons in response to visual stimulation, our understanding remains incomplete. Recent developments in retinal imaging provide promising methodologies to help assess retinal activity in the living eye. Noninvasive approaches such as in vivo imaging are critical for understanding visual function in the intact visual system and can provide longitudinal tracking of retinal function in both healthy and diseased eyes. This is particularly important for investigating changes during development, aging, disease progression, and treatment.

jhunter@ur.rochester.edu,.

1.1. Function of the Retina

The retina is a multilayered structure that detects light, processes the subsequent signals, and transmits that information to the brain (see the sidebar titled Overview of Retinal Structure). Light that enters the eye passes through the anterior optics and transparent neural retina before reaching light-detecting photoreceptors. Photon absorption by rod opsin (rhodopsin) or cone opsin (photopsins) initiates two processes: phototransduction and the visual cycle. Phototransduction is a cascade of events within a photoreceptor that amplifies and propagates the light response within a single receptor to postreceptoral cells via modulation of photoreceptor glutamate release at the synaptic terminal. In response to light, the photoreceptor becomes hyperpolarized, leading to a reduction of glutamate release at the synaptic terminal in the outer plexiform layer. This information is processed and relayed through inner retinal neurons before leaving the eye en route to the brain. In parallel, the visual cycle, also known as the retinoid cycle, recycles the chromophore through the retinal pigment epithelium (RPE) or Müller cells (for more detail, see Section 3). Combined, these processes result in retinal function with exceptionally high metabolic activity. The retina has the largest oxygen consumption by weight of any tissue in the human body (Lennie 2003, Wong-Riley 2010, Yu & Cringle 2001), requiring a substantial network of retinal vasculature to meet this oxygen demand. Therefore, biomarkers associated with phototransduction, the visual cycle, and neuro-glial metabolism have been common imaging targets for extracting retinal function.

1.2. Scope

In this review, we define retinal function as the response of the retina to light stimulation: the stimulus-evoked response. Function includes blood flow, production or removal of certain molecules within a cell, electrical activity, and cellular metabolism related to the eye's natural sensory stimulus—visible light. We restrict this review primarily to measures of vertebrate retinal function that can be observed using imaging techniques that measure retinal activity using reflected, scattered, or fluorescence light. In addition to imaging using light, we also consider several important contributions of imaging using magnetic resonance imaging (MRI). We do not cover psychophysical testing or nonimaging measures of retinal function such as electroretinograms (ERG), nor do we examine measures of visual processing beyond the retina.

2. OPTICAL COHERENCE TOMOGRAPHY

2.1. Theoretical Concept

Retinal responses to light can be measured with optical coherence tomography (OCT), an interferometric optical method for measuring light scattering in biological tissues that has exceptional axial resolution and is widely used in the ophthalmology clinic. The most robust functional signals appear to come from rod and cone photoreceptors, and recent studies show smaller signals from inner retinal layers, possibly the inner plexiform layer (Yao & Wang 2015). Although retinal light scatter in response to visual stimulation has been measured for many years with in vitro preparations (Hofmann et al. 1976), experiments have been carried out in the living eye in recent years and have provided comparative results from a wide range of species including mouse (Thapa et al. 2017, Zhang et al. 2017), tree shrew

(Erchova et al. 2018), macaque (Suzuki et al. 2013), and human (Lu et al. 2017). These rapid advances were fostered by technical advances in OCT methods that improved the resolution of imaging (Kocaoglu et al. 2016, Lu et al. 2017) down to just a few micrometers, decreased the blurring produced by eye movements via more rapid scanning (Thapa et al. 2017, Yao & Wang 2015), and increased the signal contrast of imaging via improved analysis (Thapa et al. 2017).

2.2. Fluctuations in Photoreceptor Length Measured with Optical Coherence Tomography

The axial resolution of OCT makes it possible to measure variations in the optical path length and, thus, changes in thickness of individual retinal layers. In humans presented with a liquid-crystal display with a distinctive spatial visual stimulus, the optical path length of the photoreceptor outer segments in the stimulated regions peaked at ~300 ms after a 50-ms stimulus (Figure 1a) and returned to baseline within ~3 s (Hillmann et al. 2016). This effect was much more pronounced and long-lasting after a 500- or 3,000-ms stimulus. Extending this approach to the difficult study of functional responses of human inner retinal neurons, Pfäffle et al. (2018) demonstrated various methodological advances that make ganglion cell responses measurable. Use of similar spatial patterns will be valuable in future studies that look for reginal alterations in visual response across the retinas of patients.

The use of adaptive optics (AO) combined with OCT has made possible in vivo measurements of the lengths of individual cones. Kocaoglu et al. (2016) studied hundreds of cones in humans by capturing AO-OCT images every 3 min for a 90-min period. At times, the COST image disappeared for several minutes (Figure 1b), and when it reappeared, the outer segment length was shortened, suggesting disc shedding. Duration of the loss of COST varied widely from less than 3 min up to approximately 60 min, and outer segment length decreased from 25.1 μm to 22.7 μm, a difference of approximately 9.6%. The rate of disc shedding in cones was maximal in the morning, decreasing in the afternoon and further in the evening.

Both outer segment elongation and increased light scattering were observed in mice in response to brief presentations of intense light (Zhang et al. 2017) (Figure 1c,d). The time course of light-scattering increase and outer segment elongation were highly correlated, suggesting the former was due to the latter. The authors constructed a model of how osmotic changes in outer segment elongation would affect backscatter and concluded that axial changes in the length of outer segments were sufficient to produce the observed scatter alterations. They also observed both scattering increase and outer segment changes only in control mice and not in mice lacking the rod G protein alpha subunit, indicating that phototransduction is critical to both outer segment elongation and scattering increase. In human subjects exposed to a large-field (40°) bright flash (1–12-ms duration), Lu et al. (2017) measured a very fast (less than 20-s measurement interval) increase in the distance from the inner segment/outer segment junction (or ellipsoid zone) to the cone outer segment tip (COST), which was most pronounced near the fovea where cones are the primary photoreceptors. A much slower thickness increase was observed between ellipsoid zone and rod outer segment tip, lasting until approximately 25 min after the flash (Figure 1e). The observed changes in outer retinal thickness were strongly correlated with the time course of

rod and cone dark adaptation measured psychophysically for 30 min after stimulation (Figure 1e).

2.3. Functional Responses of Inner Retina Measured with Optical Coherence Tomography

Despite growing consensus that dramatic scattering signals from photoreceptor layers are related to physical changes in the outer segments, the neuronal mechanism of the subtler light-induced alterations in the inner retina (Pfäffle et al. 2018) remains controversial. Two studies suggest a possible role for retinal ganglion cells in these responses: Mihashi et al. (2011) found no difference in inner retinal effects elicited by transcorneal or optic chiasm stimulation, suggesting both reflected a ganglion cell response. Blocking synaptic transmission with tetrodotoxin eliminated scatter responses in the inner retina, suggesting a role for retinal ganglion cells. More recently, Erchova et al. (2018) imaged inner retinal responses with OCT in anesthetized and paralyzed tree shrews in response to intense brief flashes of light as well as drifting gratings. Visual stimulation caused positive and negative changes in reflectance and increased variability of responses in the ganglion cell layer. This increased variation persisted when spatially filtered to the size of ganglion cells to remove speckle. Furthermore, these responses were correlated with on- and offset of visual stimuli, suggesting a possible origin from ON and OFF center ganglion cells, which also show responsivity to on- and offsets of stimuli in electrophysiology experiments.

A previous study of functional responses in mouse inner retina (Zhang et al. 2015) was recently improved via adoption of an analytical approach to increase the signal-to-noise ratio. Applying a method initially developed to improve vascular OCT imaging (Jia et al. 2015), Thapa et al. (2017) split the 104-nm-wide OCT signal into four slightly overlapping bands and analyzed each band separately. The intensity values in different spectral bands differed greatly, sometimes in sign, and averaging reduced overall signal, demonstrating independent functional signals in different spectral bands. This analysis made visible inner retinal change (Figure 1f). In addition to the strong scatter signals in the outer retina, there is a subtle signal in the inner plexiform layer. The magnitude of this inner retinal response was much greater than when measured previously with the full-spectrum OCT signal.

2.4. Future Developments

OCT methods for measuring retinal function look very promising given two continuously advancing features, exquisite axial resolution and high imaging speed that freezes eye motion. If combined with AO, OCT can observe effects within individual photoreceptors, even separating rods and cones (Wells-Gray et al. 2018), making detection of microscopic events such as disc shedding possible (Kocaoglu et al. 2016). An all-optical method (Ling et al. 2018) is also being developed to detect individual action potentials of cells by measuring phase changes possibly caused by membrane deformation. If it can be extended to in vivo retinal imaging, this method could revolutionize retinal function studies in humans. Because OCT needs no external contrast agent, this method is ideal for examining human retinas. A major limitation is that it cannot provide fluorescent information such as autofluorescence and biosensor-added fluorescence (see Sections 3.4 and 7.1). However, the development of joint-registered fluorescence and OCT imaging (Yuan et al. 2010) will eventually provide the multimodal benefits of both approaches.

3. RETINAL DENSITOMETRY

3.1. Theoretical Concept

Photoreceptor outer segments contain photopigments that absorb photons of light and begin the phototransduction process. These photopigments are comprised of an opsin that dictates the spectral sensitivity of the photopigment and the chromophore 11-*cis*-retinal. In the dark, photoreceptor outer segments are packed with tens to hundreds of millions of photopigment molecules that are ready to absorb photons in the visible spectrum (~400–700 nm). Photopigment molecules are activated when exposed to light, but upon releasing the chromophore, they are unable to absorb additional visible wavelength photons. The opsin does not strongly absorb in the visible spectrum without retinal. Light-induced change in the spectral absorption of the photopigment is known as bleaching. Spectral absorption of photoreceptors differs depending on available photopigment. Retinal densitometry takes advantage of this change in spectral absorption to measure photoreceptor pigment density. The pigment optical density is measured by comparing the intensity of reflected visible light in response to a bright visible light bleach and the amount of photopigment inferred (Figure 2a). Tracking the optical density over time during bleach recovery can provide information about the rate-limited kinetics of pigment regeneration (Lamb & Pugh 2004). Furthermore, bleaching with specific wavelengths tuned to the preferred wavelengths of different cone classes can be used to probe and identify individual cone spectral types (Roorda & Williams 1999).

3.2. Classical Rhodopsin Densitometry

Campbell & Rushton (1955) performed early work in retinal densitometry measurements using modified retinal cameras. Since then, the introduction of new imaging modalities including scanning laser ophthalmoscopes (Elsner et al. 1992, van Norren & van de Kraats 1989) and AO imaging systems (Masella et al. 2014) has made possible new measurements. Densitometry measurements have provided consistent results regarding the photosensitivity of rhodopsin from rods. For example, photosensitivity (expressed in units of scotopic illuminance) has varied between 6.9 in Rushton's (1956) data and 7.2 in Morgan & Pugh's (2013) data. Measurements of the rate of rhodopsin regeneration in humans are also consistent across densitometry experiments and with psychophysical and ERG results (Lamb & Pugh 2004).

Possibly owing to reduced reflection from peripheral cones, which have short tapered outer segments and decreased reflectivity at their narrow tip, Morgan & Pugh (2013) found an absence of cone contributions in human subjects at an eccentricity of 15°. This is also near the eccentricity of maximum rod density. Similarly, using an AO scanning light ophthalmoscope (AOSLO) for macaques, Masella et al. (2014) found no significant difference in apparent density or initial photopigment recovery rate at ~15° eccentricity when the contribution from cones was removed.

Despite their theoretical utility, densitometry measurements have been fraught with challenges in accounting for non-photopigment-related variations in sequentially acquired images in bleached and unbleached states. These measurements likely do not represent

complete double-pass transmission through the photoreceptor, as multiple reflections and absorptions can occur from pre- to post-receptor retinal layers (van de Kraats et al. 1996). Generalized models of fundus reflectance can be incorporated into analyses of densitometry data (Morgan & Pugh 2013, Masella et al. 2014). Additionally, a normalization has also been applied with images taken at a wavelength likely unaffected by a change in pigment density (Morgan & Pugh 2013). This works well in widefield images of the peripheral retina where the contribution of cones in minimal, but it is not successful in cone-dominated fovea or in AO imaging methods (DeLint et al. 2000, Masella et al. 2014).

Densitometry measurements may provide valuable information about photoreceptor function in healthy and diseased eyes. With age, the difference between bleached and dark-adapted photopigment density increases, and the rate of rhodopsin regeneration declines (Liem et al. 1991). Many diseases, such as fundus albipunctatus, vitamin A deficiency, and drusen in early age-related macular degeneration, manifest with reduced pigment density and/or slowed dark adaptation (Liem et al. 1996). No disorders with accelerated dark adaptation have been documented. Using an AOSLO to perform retinal densitometry measurements in macaque, Masella et al. (2014) observed changes in the rhodopsin density of rods that were located above regions of RPE photodamage, but the initial recovery rate remained unchanged. Thus, these photoreceptors retain a functioning visual cycle, even in the presence of RPE disruption.

3.3. Densitometry for Cone Classification

Using AO imaging, the photopigment density of single cones can be separated from that of rods. Using AO fundus photography with selective comparisons between dark-adapted and bleached states, Roorda & Williams (1999) and then Hofer et al. (2005) classified individual cones. Their early work represented a time-consuming process that could require repeated daily sessions for up to 5 days for each bleaching condition. Today, with the development of high-speed retinal tracking algorithms in combination with AOSLO, such measurements may be performed with intermittent imaging over the course of 3–9 h. Sabesan et al. (2015) performed cone-resolved densitometry with AOSLO (Figure 2d) by first dark-adapting subjects for 5 min. S cones were identified by simultaneously bleaching and imaging at 543 nm. Light at 680 nm was used to bleach L cones ~15 times more than M cones, and 479 nm light was used to selectively bleach M cones ~ 1.8 times more than L cones. Intensity versus time was tracked for a 3 s video acquisition, so the relative total change in reflected intensity could provide an indication of the amount of bleaching. For example, at 543 nm, S cones showed little to no response, whereas L/M cones showed a substantial increase in reflected intensity. Using this method, Sabesan et al. (2015) reported that their optical densities are comparable with those of other groups, but lower than those estimated from single-pass psychophysical measurements. Such optical measurements can be the basis for psychophysical testing to understand the perceptual responses of single-cone stimulation (Sabesan et al. 2016). Furthermore, cone classification may be important in identifying the susceptibility of various cones to phototoxicity or retinal degeneration

Bedggood & Metha (2012) investigated the millisecond dynamics of visible light reflectance of individual foveal cones following bleach. By combining densitometry with a flood-

illuminated AO ophthalmoscope, they found substantial variability between individual cones within 1° of the fovea in response to light adaptation to a supercontinuum laser source in the range of 540 nm to 573 nm. With a rate of 1,000 frames/s, fluctuations were observed on the order of milliseconds. The observed cone-to-cone variability in the magnitude of the reflected intensity increased, suggesting that as cone photopigment becomes bleached optical waveguiding improves. Individual cones within the same putative color class produce heterogeneous responses to the same stimulus, showing significant variability in photopigment density and photosensitivity between neighboring cones.

The varied spectral sensitivity of rods as well as S, M, and L cones can also be used to map the cone mosaic near the fovea or to perform widefield assessments of photoreceptor densities. Tracking reflectance in response to light adaptation at different wavelengths over time in rhesus monkeys, Hanazono et al. (2012) measured M/L, S, and rod functional maps across the central 20° (Figure 2c). By selecting various time points for comparison, they isolated the responses of rods and different cone classes. M/L cone density and S cones were assessed by plotting light-reflectance change measured 60–180 s and 30–60 s after the onset of 590 and 445 nm light, respectively. Rods were also assessed using adaptation to 500 nm light with responses between 52.5 s and 150 s. The time windows for analysis were chosen on the basis of inflections in the percentage change in light reflectance versus time for cone-rich foveal regions and rod-dominated temporal retina. These functional maps are comparable to photoreceptor density maps that take into account how photoreceptor volume varies with eccentricity. However, the former require very bright light exposures and long fixations. Thus, this methodology is not ideal for use in humans.

3.4. Using Fundus Autofluorescence for Retinal Densitometry

Photopigment density may also be inferred from the increase in autofluorescence intensity measured in the RPE (Figure 2d). Given their accumulated lipofuscin, RPE cells fluoresce from the deepest retinal layers, and exposure to visible photopigment bleaching lights reduces absorption of screening photopigment. Thus, as Theelen et al. (2008) demonstrated using a Heidelberg scanning laser ophthalmoscope, the intensity of autofluorescence emitted from the RPE increases following photopigment bleaching (Prieto et al. 2005). Morgan & Pugh (2013) found the initial increase in autofluorescence after a full bleach of rhodopsin is significantly greater than predicted by rate-limited kinetics of rhodopsin regeneration and possibly reflects a different component of retinoid processing. This raises the question of whether the same apparent measurement is confounding two processes. This autofluorescence method provides single-pass measurements, potentially explaining why the optical density measurements it produced were lower than traditional densitometry measurements (Prieto et al. 2005). Although potentially clinically useful, such densitometry measurements are time consuming and confounded by competing signals, so they have not been adopted. Autofluorescence densitometry may also be challenging or impossible in the presence of RPE atrophy, yet a recent report by Choi et al. (2017) demonstrates utility in patients with acute central serous chorioretinopathy.

4. INTRINSIC SIGNAL IMAGING

4.1. Concept

Intrinsic signal optical imaging encompasses various techniques reporting functional activity on the basis of endogenous changes in tissue. Comparison of images from baseline and stimulated states reveals tiny changes in optical back reflection are often present but invisible to the naked eye. Sensitive digital cameras can yield repeatable imaging and quantification of these changes. There is no single biophysical origin of intrinsic signals; rather, they compose the aggregate response of multiple optical changes in response to tissue stimulation such as those of activated neurons and glial cells (Hill & Keynes 1949, Keynes 1951). These changes can alter optical properties and thus may reveal neural tissue physiology. In addition, as thirsty neurons drive local modulations in blood flow to serve metabolic needs, neurovascular coupling also impacts optical interactions with tissue.

Intrinsic signal optical imaging was originally developed to reveal functional brain architecture that could not be visualized by anatomy alone. Optical changes were confirmed to arise in neural tissue partly in response to hemodynamic modulations caused by neural activity (Frostig et al. 1990, Grinvald et al. 1986, Malonek & Grinvald 1996, Malonek et al. 1997, Ts'o et al. 1990) as well as light scatter endogenous to the neural tissue (Frostig et al. 1990). Other physiological processes such as osmotic changes or ionic movements that cross the cell membrane as well as pigment and chromophore changes associated with glycolysis or related to the redox ratios of energy production and utilization from NAD, cytochromes, or other components of the citric acid cycle may also induce optical changes (Cohen 1973, Cohen & Salzberg 1978).

Although retinal neurons share many similarities with cortical neurons, the retina contains several specialized chromophores, proteins, photopigments and epithelia that are unique. Measuring photopigment densitometry (Rushton 1956) is one such example described above. However, because mammalian opsins show dramatic absorption reduction beyond 700 nm (DeLint et al. 2000, Grieve & Roorda 2008, Stockman & Sharpe 2000), intrinsic signals in the near infrared (NIR) (~700–1,000 nm) are likely distinct from photopigment-related changes in the retina. Therefore, NIR optical changes may represent a unique class of biophysical reporters.

Intrinsic signal optical imaging in the retina compares a baseline (NIR only) with a stimulated state (NIR plus visible light, the retina's natural stimulus). This approach has at least three major benefits. First, functional measures are distinct and not confounded by photopigment density (DeLint et al. 2000). Compared with its visible densitometry counterpart, the NIR intrinsic signal often shows opposite polarity as well as a different spatial topography and functional time course (Figure 3a) (Tsunoda et al. 2004). As a result, optical signatures could be studied in cells without photopigment. Second, the use of NIR light may leave the retinal opsins in a near-dark-adapted state (Stockman & Sharpe 2000) that is beneficial for imaging the baseline and light-evoked response. Third, because NIR light is within the sensitivity range of many digital cameras, more light can be used without risking photochemical damage to the retina. Because ample photons are provided for digital detection, imaging of the signal-to-noise ratio is increased.

4.2. Spatial Characteristics of Intrinsic Signal Imaging

Using a modified scanning laser ophthalmoscope, DeLint and colleagues (2000) found a slow change in backscattered NIR light in response to visual stimulation at the fovea of the human retina. Along similar lines, Tsunoda and colleagues (2004) observed changes in NIR reflectance in response to a short flash of visible light. In contrast to the increase seen in visible light reflectance (consistent with densitometry), recordings made with bright 900-nm imaging light revealed a global decrease in NIR reflectance (Figure 3b). Compared with its visible densitometry counterpart, the NIR intrinsic signal showed not only opposite polarity, but also a different spatial topography and functional time course (Figure 3a,b).

The NIR response of the human retina can be focally stimulated (Abramoff et al. 2006). Measured with a spectrally modified flood ophthalmoscope using a patterned 550-nm visual stimulus, it was localized to the area of stimulation. Although its biophysical origins are still being elucidated, this response is evidence of a focally precise mechanism. In many studies, it could be evoked with a very-low-energy visible stimulus of only 10 cd/m^2 corresponding to the low-photopic, high-mesopic range of vision. Thus, the NIR response may be physiologically relevant to ordinary pattern vision.

4.3. Animal Studies Reveal Conserved Features of Mammalian Optophysiology in the Near Infrared

Multiple studies have used animal preparations to facilitate more detailed study, and animal studies provide opportunities for retinal stabilization that cannot be realized in humans (Schallek et al. 2009a,b). NIR optical signals have been observed in every species examined in vivo including cat (Schallek & Ts'o 2011; Schallek et al. 2009a, 2012; Ts'o et al. 2009), monkey (Hanazono et al. 2012, Ts'o et al. 2009, Tsunoda et al. 2004), rabbit (Naderian et al. 2017), mice (Wang et al. 2016), and frog (Zhang et al. 2011). Such findings point to a signal that may represent a consistent aspect of vertebrate and, especially, mammalian physiology. In anaesthetized and paralyzed cat, the spatial confinement of the intrinsic signal yielded a spatial point-spread function of ~80 μm, corresponding to 22 arcmin (Ts'o et al. 2009). Therefore, a spatially precise control mechanism may be used to probe the geographic integrity of the retina at a variety of eccentricities.

When imaged with flood-illuminated cameras, macaque monkeys and humans show a predominantly negative signal (decrease in backscatter) (Abramoff et al. 2006, Hanazono et al. 2012, Ts'o et al. 2009, Vanzetta et al. 2014). However, in some species, especially in cat, there appear to be both spatially localized negative and positive signals (increase in light reflectance). Negative signals colocalize with stimulus location, whereas positive signals are often adjacently located (Schallek et al. 2009b). The sided asymmetry of the positive signal is poorly understood, though vascular watershed indicates that vascular shunting (vascular steal) could provide a basis for both positive and negative signals (Shmuel et al. 2002). Negative and positive signals are present at the same time (Figure 3c), suggesting a more complex interaction at the spatial or axial scale. However, neither signal appears to grow or propagate spatially over time, so activity remains spatially specific and does not, for example, demonstrate traveling wave activity (Figure 3c). In cat, both negative and positive signals appear to have a similar time course on the order of seconds that may indicate a

similar biophysical origin. In rabbit, however, intrinsic signals appear to have a biphasic response exhibiting both negative and positive signals that are temporally separate. These differences prompt the question of whether there are species differences or whether laminar contributions may impose optical changes that balance inner and outer retinal contributions in different ways as the signal is integrated across the entire neural retina, RPE, and some contribution of the choroid and sclera (van de Kraats et al. 1996).

In addition to their two reflectance polarities, NIR signals exhibit two generalized time courses. Fast optical signals show kinetics on the order of milliseconds and appear to resemble the electrical response function of activated neurons when compared with components of the ERG (Wang et al. 2016, Yao & Wang 2015, Zhang et al. 2011). Slow optical changes have a rise time on the order of seconds and often have a progressive growth function consistent with retinal activation energy (Abramoff et al. 2006, Okawa et al. 2007, Schallek et al. 2009b, Tsunoda et al. 2004). Most signals reported in vivo show signal rise time on the order of seconds enabling more sensitive integration at safe light levels.

Given the differences reported above, signal origins may arise from layers containing different subsets of neurons. Attempts to address this issue are perhaps where the field is most fraught with conflicting findings. In studies from laboratories using rhesus monkey and rabbit, injection of inner retinal blocking drugs reduced the intrinsic signal amplitude (Hanazono et al. 2008, Naderian et al. 2017). However, other studies using similar drugs in cat found inner retinal blocking agents have minimal impact on the intrinsic signal amplitude, suggesting a dominant outer retinal origin (Schallek et al. 2009a) that has also been corroborated using a cat model of congenital glaucoma in which ganglion cells were severely compromised (Schallek et al. 2012). Studies using confocal AOSLO imaging also point to a signal change arising from individual photoreceptors in both frog and human (Cooper et al. 2017, Grieve & Roorda 2008, Zhang et al. 2011). Further research is needed to sort out the laminar contributions and species-related differences. Currently, the only commercially available instrument for making such measurements is the Retinal Functional Imager (Optical Imaging, Ltd., Rehovot, Israel) (Izhaky et al. 2009, Nelson et al. 2005, Vanzetta et al. 2014). Reports from this device focus mainly on blood velocity (discussed below), though some modalities reveal distinctive focal activations (Figure 3d).

4.4. Intrinsic Signal Imaging with the Aid of Adaptive Optics Ophthalmoscopes

AOSLO resolution has allowed for precise retinal motion correction to mitigate further the impact of motion artifacts that could contaminate small intrinsic optical signals. Using an AOSLO to image the response of single cones to patterned visible stimuli in human, Grieve & Roorda (2008) studied the cellular contributions of intrinsic signals related to photoreceptor function (Figure 4a). Given the confocality of the system (~150 μm), the strongest signals using 840-nm light were observed conjugate with the photoreceptor outer segments and represented slow changes on the order of seconds. This finding is similar to pharmacological studies that emphasized an outer retinal origin (Schallek et al. 2009b). However, in contrast to much work in primate and cat, the photoreceptor-based intrinsic signal appeared to be an increase in reflected light. Stockman & Sharpe (2000) ruled out a primary contribution from photopigment densitometry because the absorption coefficient of

photopigment at 840 nm given the power intensities used was negligible. This study did not detect a spatially correlated negative signal. However, using single-receptor resolution, Cooper et al. (2017) distinguished both positive and negative polarity intrinsic signals in response to visible stimulation. The authors also found that photoreceptors demonstrated both positive and negative signals at the single-cell level in response to the same stimulation (Figure 4b). The aggregate response was assigned a variance measure rather than the fractional reflectance change measure used by others. Receptor reflectance variances are sensitive to light of different wavelengths in a manner that tracks the human spectral sensitivity function (V_λ), suggesting the same processes that initiate our vision also modulate the optical signature (Figure 4d). Work remains to determine why cone reflectance both increases and decreases in response to the same visual stimulus.

4.5. Contributions from Retinal Blood Flow

Findings from several studies support the idea of a hemodynamic optical signal in the retina. For example, when contrast agents were injected systemically into blood circulation, NIR intrinsic signals increased in magnitude (Schallek & Ts'o 2011) while maintaining a similar spatial scale and matched temporal dynamics. Thus, intrinsic signals arise, at least partly, in response to changes in blood flow in the retina, consistent with numerous brain studies (Malonek & Grinvald 1996, Malonek et al. 1997). Spatial stimuli also appear to activate an optical change in feeding and return vessels far from the visual stimulus (Figure 5c). Optic disc analyses show darkening of the primary arterioles and venules (Hanazono et al. 2007) and vessels projecting to the visually stimulated area (Okawa et al. 2007). Combined, these studies suggest that modulations in retinal blood flow may change how NIR light interacts with the retina, despite low overall absorption of hemoglobin at these wavelengths.

5. BLOOD FLOW IN THE RETINA

5.1. Concept

Blood perfusion is essential for healthy vision. It is the source of retinal nutrition and is critical for removing metabolic waste products. Two primary circulation pools serve the retina: the choroidal complex, located behind the neural retina, and retinal circulation, located on the surface and interspersed within the inner retinal layers in human and other holangiotic retinas (Michaelson & Friedenwald 1954).

Since the observations of Roy & Sherrington (1890) more than a century ago, coupling between neural activity and blood flow (neurovascular coupling) has provided a physiological linkage enabling noninvasive readout of neural tissue via patterns of blood flow and oxygen saturation. As such, neurovascular coupling is a fundamental readout mechanism in blood-oxygen-level-dependent (BOLD) functional MRI (fMRI), laser Doppler imaging, and aspects of the intrinsic signal response discussed above. In the brain and retina, changes in both total blood flow and oxygen content of hemoglobin are modulated in response to the activity of functionally organized neural populations (Fox & Raichle 2007, Ogawa et al. 1990; for comprehensive reviews of neurovascular coupling mechanisms in the retina, see Kornfield & Newman 2014, Newman 2013).

5.2. Oximetry

The first spectral measurements of blood were performed in the late 1800s by Stokes (1863), who determined the spectral characteristics of oxygen-bound and -depleted hemoglobin. Spectral changes associated with oxy- and deoxyhemoglobin have been extensively characterized, and initial attempts to measure oxygen anteriovenous oxygen unloading have been visualized in the human eye. Retinal circulation in human shows an anteriovenous saturation difference of approximately 35–43% (Hickam & Frayser 1966, Schweitzer et al. 1999) that is consistent with the high metabolic demands of the neural retina (Ames et al. 1992, Lennie 2003, Wong-Riley 2010). Oximetry is not considered a strong intrinsic signal contributor in the choroid, owing to the exceptionally high perfusion rate of ~1% total oxygen extraction measured in cat (Alm & Bill 1970).

Today, several commercial and research-grade devices including the Oxymap T1 (Reykjavik, Iceland) and Retinal Functional Imager measure oximetry in the largest vessels within retinal circulation (Blair et al. 2017, Geirsdottir et al. 2012, Izhaky et al. 2009, Nelson et al. 2005). Challenges remain in properly accounting for pigmentation, scatter, and spectral properties of the anterior optics that may alter or bias spectral measurements and degrade the integrity of the oximetric signal (Beach et al. 1999). There is also a limit to the test-retest variability of fundus-based measurements in the same subjects over weeks (10–16%) and within the same session (3.7–8%) (O'Connell et al. 2014) Nevertheless, oximetry may reveal baseline dysregulation in diseased retinas (Stefansson et al. 2017).

Another approach that obviates the need for optical pigmentary corrections is fMRI (Ogawa et al. 1990), which has revealed both blood flow and BOLD hemodynamics associated with neural activity. Neurovascular coupling is the key readout mechanism used in BOLD fMRI, as changes in total blood flow and oxygen content of hemoglobin are dependent on total hemoglobin levels and blood oxygen content (Fox & Raichle 2007, Ogawa et al. 1990). Technical advances have also minimized voxel size to enable laminar images of the retina (Duong 2014, Duong et al. 2002). In studies by Duong and colleagues (2002), retinal hemifield stimulation caused focal stimulations in putative blood flow changes (Figure 5a). These changes represent blood volume or BOLD signals, as has been corroborated by gas challenge experiments where subjects breathe different concentrations of oxygen, carbon dioxide, and nitrogen affecting systemic blood gases and revealing modulated BOLD responses (Peng et al. 2011, Zhang et al. 2011).The time course of fMRI findings show some consistency with optical measures of putative blood flow changes of the intrinsic signals (discussed above) (Shmuel et al. 2002). Currently, fMRI retinal imaging is time-consuming, expensive, and not available to many research institutions. Nevertheless, these early investigations offer great potential for understanding blood flow regulation in healthy and diseased eyes.

5.3. Imaging Stimulus-Evoked Blood Flow Changes

Several decades of work have revealed that retinal circulation modulates blood flow in response to visual stimulation and blood flow states may differ in light- versus dark-adapted retinas (Feke et al. 1983). Investigations using high-resolution AOSLO have measured the speed of single blood cells (Guevara-Torres et al. 2016; Martin & Roorda 2005, 2009; Tam

& Roorda 2011; Zhong et al. 2012). Zhong and colleagues (2012) showed that the velocity of single blood cells in larger arterioles increased in response to visual stimulation. Large retinal subfields (2°–10° visual angle) also modulate their local blood flow in response to visual stimulation (Figure 5b). These findings are consistent with the neurovascular coupling response reported in the brain. Work remains to determine the degree of local control in the retina and which cell type regulates this control (e.g., smooth muscle or retinal pericytes) (Schallek et al. 2013).

Techniques measuring Doppler shift in light revealed that blood cell speed can also be extracted to provide a meaningful report of blood velocity in larger vessels (Feke & Riva 1978, Riva et al. 1972). Along with visual stimulus flicker and a constant light-adapted state, blood flow increase is also observed in retinal circulation (Riva et al. 1991, Vo Van & Riva 1995). Initial reports used a single beam positioned on a vessel of interest, and this approach was subsequently coupled with OCT methods (Leitgeb et al. 2014, Singh et al. 2010). Reports using Doppler signals to reveal flicker-evoked responses show increased blood velocity, flow, and volume (Wang & Kefalov 2011). Combining OCT, Doppler shift, and dynamic vessel analysis, Garhöfer et al. (2004) estimated substantial increases in total blood flow to the retina exceeding 50% following visual flicker stimulation. An increase in retinal vessel diameter and, as a consequence, lower resistance and faster blood velocity mediate the change in total blood flow. Work on this front is beginning to study the impact of neurovascular dysfunction in a number of retinal degenerative diseases using the Dynamic Vessel Analyzer (Imedos GmbH, Jena, Germany), which measures large vessel diameter in response to visible flicker (Garhöfer et al. 2010). Analyses will benefit from combining measures of diameter alone with those of blood cell speed (Riva et al. 1991, Vo Van Toi & Riva 1995, Zhong et al. 2012) or of the flux of single blood cells recently demonstrated using labeled (Kornfield & Newman 2014) and label-free detection of single blood cells (Guevara-Torres et al. 2016).

6. INTRINSIC FLUORESCENCE IMAGING

6.1. Theoretical Concept

The generation of adenosine triphosphate, a unit of intracellular energy, is of critical importance for cell function. In the mammalian central nervous system, its generation takes place mostly through either glycolysis (anaerobic) in the cytosol or the Krebs cycle (citric acid cycle or tricarboxylic acid cycle) and oxidative phosphorylation (aerobic) in the mitochondria. In these cycles, oxidation and reduction reactions involve nicotinamide adenine dinucleotide (NADH) and flavin adenine dinucleotide (FAD) (Wong-Riley 2010). NADH and FAD are fluorescent, potentially providing a window into cellular respiration throughout the entire retina (Heikal 2010, Huang et al. 2002).

The visual cycle is critical for maintaining human vision. Following photon absorption by photopigment in the photoreceptors, the chromophore 11-*cis*-retinal is isomerized to all-*trans*-retinal, which must be converted back into 11-*cis*-retinal to rebind with the opsin through the visual cycle (Kiser et al. 2012). To begin this process, all-*trans*-retinal is converted into all-*trans*-retinol in the photoreceptor outer segments. All-*trans*-retinol is moved into the cells of the RPE, where it is converted into all-*trans*-retinyl esters that are

stored in retinosomes until needed. All-*trans*-retinyl esters are then converted into 11-*cis*-retinol and finally to 11-*cis*-retinal. The latter is transported to the photoreceptor outer segment to bind with the opsin, concluding the visual cycle. This entire process of photopigment regeneration can be quite slow; a completely bleached human rod can require 30 min or more to regenerate all its photopigment (Hecht et al. 1937).

In addition to using the traditional visual cycle for chromophore regeneration, cones can regenerate photopigment through a cycle involving Müller cells (Wang & Kefalov 2011). In this alternate cone cycle, all-*trans*-retinol is transported to Müller cells where it is converted into 11-*cis*-retinol before being transported back to the cones. Unlike rods, cones can convert 11-*cis*-retinol into 11-*cis*-retinal. This alternate process is significantly more rapid at producing the 11-*cis*-retinal required for binding with the opsin to form cone photopigment. Advantageous for imaging, molecules involved in the visual cycle, in particular, retinol and retinyl ester, are highly fluorescent. By-products of the visual cycle that accumulate in the RPE form lipofuscin granules, which are also fluorescent. However, because lipofuscin does not vary in response to patterned light stimulation, it is outside the scope of this review.

6.2. Imaging Cellular Metabolism

Ex vivo studies indicate metabolism changes in response to visual stimulation (Chen et al. 2005). FAD in retina can be imaged in vivo via blue-light excitation (Elner et al. 2008). The magnitude of emitted flavoprotein fluorescence varies with disease (Field et al. 2012), but it has not been studied in response to visual stimulation. To image NADH, traditional single-photon fluorescence excitation must use UV light. However, UV light is highly phototoxic, and it is strongly filtered through the anterior optics of primate eyes because its peak excitation falls below 400 nm, which is poorly transmitted by the optics. By contrast, two-photon excitation uses longer-wavelength pulsed light that can pass through the anterior optics and reach the retina to produce an excitation approximately equivalent to half the wavelength or twice the energy. NADH may be the dominant fluorophore in fluorescence images of retinal ganglion cells and other inner retinal neurons acquired in macaque (Sharma et al. 2016b). By comparing the intensity of fluorescence emitted by FAD and NADH, researchers can quantify changes in the reduction-oxidation (redox) state of a cell (Chance et al. 1979). Such measurements are feasible, but challenging, in vivo and have not yet been demonstrated in the living eye (Miura 2018).

6.3. Imaging the Visual Cycle

Retinoids of the visual cycle also require two-photon excitation for visualization in the living primate eye. Sharma et al. (2016a) observed retinol production in macaque rods and cones, retinol clearance, and establishment of an equilibrium in response to light adaptation. Following a brief incremental stimulation, the magnitude of retinol production and the rate of its clearance from the outer segment can be measured in macaque rods (Sharma et al. 2017) (Figure 6a,b). The fractional change in emitted two-photon excited fluorescence (TPEF) as a function of the intensity of incremental stimulation was consistent with the fraction of bleached rhodopsin pigment.

However, the rate of retinol clearance from rods is substantially faster than rates measured by densitometry, which rely on the regeneration of visual pigments. Imaging the visual cycle may be useful in quantifying photoreceptor function, as demonstrated in three macaque models of altered outer retinal function. In a macaque model of induced retinal degeneration, photoreceptors missing their outer segments showed little change in TPEF upon stimulation (Walters et al. 2019) Similarly, phototoxic damage to select cones may be identified by a cell-specific decrease in TPEF intensity and altered TPEF time course after visual stimulation (Schwarz et al. 2018). The rate at which TPEF intensity changes with visual stimulation is also slowed in the cones of macaques breathing 10% versus 100% O_2. (S. Walters & J.J. Hunter, unpublished data). In mouse, TPEF imaging of the RPE revealed retinosomes that sequester retinyl esters until needed to regenerate photopigment. In response to visual stimulation, there was an increase in TPEF intensity of the retinosomes corresponding to an increase in the concentration of retinal esters (Imanishi et al. 2004) (Figure 6c). Translating these TPEF measurements of the visual cycle (Schwarz et al. 2016) may be greatly beneficial in identifying the early stages of human retinal degeneration involving an altered photoreceptor visual cycle such as Stargardt's disease, retinitis pigmentosa, or age-related macular degeneration.

7. MONITORING NEURONS WITH EXTRINSIC FLUORESCENT BIOMARKERS

7.1. Theoretical Concept

The precise metabolic and physiological status of retinal neurons can be tracked by measuring fluorescent signals emitted by biosensors targeted to cells and properties of interest. This is already a highly developed technology for use ex vivo or in other organ systems for monitoring neural activation (calcium indicators, voltage sensors, glutamate markers), metabolism (glucose level, pH, mitochondrial function, hypoxia), as well as gene expression. Much of the early use of fluorescent biomarkers was with in vitro preparations (Duebel et al. 2006, Wang et al. 2014), since in vivo imaging can be difficult, but over time increasingly more studies have developed methods for in vivo imaging involving choice of optimal organisms (e.g., larval *Xenopus* or *Drosophila*) and methods adapted to a variety of larger organisms, such as AO imaging. Genetically encoded biosensors (e.g., GCaMP) can be particularly valuable in providing stable, long-term monitoring, although less permanent indicator dyes (e.g., Oregon green 488) can be inserted repeatedly into cells. Choice of indicator is critical, and considerations include whether the indicator provides a quantitative metric (e.g., a ratiometric signal or FLIM) and minimizes measurement uncertainties due to uneven dye loading, photobleaching, cell density, etc. Sensors should be selectively targeted to the cells or cell components of interest (amacrine versus bipolar cells, different classes of horizontal or ganglion cells). It is also important to determine the acute or long-term toxicity of the sensors or the light used to image the targets as well as whether the sensor alters the function being assessed or if its signal is altered by changes unrelated to the measure of interest (for example, pH alters some biosensor signals). Because the retina, unlike the brain, is optically transparent, it may be used to image fluorescent signals in deep tissue without the severe attenuation and scattering produced by brain tissue.

7.2. Biomarkers of the Metabolic State of Retinal Neurons

Given the similarities between brain and retinal neurons, many metabolic biomarkers developed to examine the former (Nguyen et al. 2017) may be applied to retinal studies (Stefansson et al. 2017). The most extensive research, including much in vivo imaging, has been done with fluorescent biomarkers of retinal oxygenation or reactive oxygen species. To date, these methods have been used to examine many retinal manipulations including reperfusion injury after elevation of interocular pressure (Rayner et al. 2014), light damage (Prunty et al. 2015), hypoxia (Uddin et al. 2016), retinal vein occlusion (Uddin et al. 2017), and nerve crush (Fan et al. 2017). In future, these approaches may be applied to study light-evoked vascular activity as described above for nonfluorescent methods. Quantitative fluorescent biomarkers for such neuronal indexes as glucose, pH, redox ratio, NADH, etc., are also being developed (Yellen & Mongeon 2015) for ratiometric or lifetime imaging, but they have not been used in in vivo studies.

7.3. Imaging Indicators of Neural Function

Many biomarkers can track neuronal function, providing complementary information about neuronal activity. Neuronal function was traditionally measured with electrophysiology, including recordings of extracellular neuronal spiking as well as intracellular and local field potentials measuring excitatory and inhibitory slow potentials. Mimicking electrophysiology, some imaging methods examine membrane or dendritic voltage (Hochbaum et al. 2014, Maclaurin et al. 2013, Xu et al. 2017), calcium levels that increase within excited neurons (Thestrup et al. 2014), neuronal glutamate release (Borghuis et al. 2013, Park et al. 2014), and chloride concentration (Zhang et al. 2006). These measures can be precisely related to excitatory and inhibitory neuronal inputs as well as the impact of neuromodulators such as dopamine, acetylcholine, and histamine. In vitro assays have been used to develop fluorescent markers of neuronal function to understand neuronal function, providing an important first step toward in vivo application.

However, when findings depend on the intactness of the organism, in vivo studies are necessary. Combining in vitro and in vivo methods, one study demonstrated that internal stores of calcium contribute little, if anything, to the light response of *Drosophila* ommatidia, which depends on influx of extrinsic calcium (Asteriti et al. 2017). Calcium responses were imaged with the fluorescent sensor GCaMP6f expressed in photoreceptors of transgenic *Drosophila* under the control of the opsin promoter Rh1. Measurements were made in dissociated ommatidia in calcium-free medium and compared with whole-cell patch-clamp electrophysiological recordings as well as in vivo imaging to exclude the possibility that dissociation altered ommatidial response.

Calcium imaging with an AOSLO has been used to measure the light responses of retinal ganglion cells in mouse and macaque retina, an approach complicated by potential cross talk between the visual stimulus and the visible imaging light. In an initial study to insert GCaMP3, (Yin et al. 2013) injected a glycoprotein-deleted rabies virus (Wall et al. 2010) into mouse superior colliculus for retrograde transport into mouse retinal ganglion cells. Interference between stimulating and imaging light sources was minimized by separating their spectral absorption, a method previously described by Akerboom et al. (2013). Yin and

colleagues (2013) altered this method by stimulating photoreceptors with a highly visible ultraviolet light (Nikonov et al. 2006) that minimally activates GCaMP. ON and OFF responses were observed in different ganglion cells; certain cells responded to 8-s stimuli with a sustained response (Figure 7a), whereas others showed a more transient response. This study (Yin et al. 2013) demonstrated a major benefit of in vivo fluorescence imaging—the ability to image the same cell repeatedly over multiple days. Indeed, the cellular visual response decreased before they could no longer be imaged. Calcium responses may also be measured with infrared light and TPEF (Bar-Noam et al. 2016). Using a modified two-photon microscope, Bar-Noam and coworkers (2016) found that GCaMP6s-labeled ganglion cells responded robustly to repeated visual stimulation of 10–20-ms pulses of blue (~450–500 nm) light.

AOSLO imaging of calcium sensors have been used to measure retinal ganglion cell responses in living macaque (Yin et al. 2014) (Figure 7b). The spatial separation between foveal photoreceptors in macaque and the ganglion cells to which they project minimized cross talk between the stimulating and measuring light. Calcium indicator was inserted into the inner retinal neurons via intravitreal injection of AAV2-CAG-GCaMP5, which was densely expressed in a circular band around the fovea. As in mouse studies, Yin et al. (2014) identified both ON and OFF ganglion cells, 12 of whose intensity response function they also measured. Subsequently, measurements using GCaMP6s and fine-flickering checkerboard stimuli have shown individual macaque ganglion cells are radially displaced approximately 200 to 400 μm from their foveola receptive fields (Figure 7c) (McGregor et al. 2018).

Measurements of calcium responses provide a unique way to examine directly optogenetic vision restoration in blind mouse by the use of the red-shifted channelrhodopsin ChrimsonR, developed by Klapoetke et al. (2014). Individual ganglion cells of retinal degeneration (RD10) mice were coinjected with viral vectors containing both ChrimsonR and the calcium indicator, and many cells in the ganglion cell layer then expressed both constructs (Cheong et al. 2018). Cross talk was minimized via ultraviolet visual or red ChrimsonR stimulation, neither of which stimulated GCaMP. The amplitude of restored responses decreased slowly over a period of approximately 6 weeks, possibly owing to changes in ChrimsonR, GCaMP6, or both.

In a major advance for in vivo functional imaging, Yang et al. (2016) used calcium and voltage indicators to examine the light responses in the first few neurons of the drosophila visual pathway (comparable to bipolar and ganglion cells in vertebrates). Voltage responses were essentially identical to patch-clamp electrophysiology of the same neurons, and different locations along the same neuron showed consistent results. Changes in the sign, amplitude, and kinetics of responses were found only across synapses. However, calcium responses varied substantially from location to location within a single neuron, indicating compartmentalization of local processing and making it possible for a single neuron to transmit distinctive signals across different synapses. Application of both sensors provided valuable insights into slow potentials as well as neuronal spiking. Prospects for the use of extrinsic fluorophores to measure neuronal metabolism and function are promising. Because many available biomarkers can be conjugated to a fluorescent marker and given the very

distinctive lifetimes of different fluorophores, future approaches may provide intensive or ratiometric fluorescent readouts (Stepanenko et al. 2008).

8. CONCLUSIONS

As the only portion of the central nervous system that is optically accessible, the retina may be used to examine function longitudinally in animals and to carry out noninvasive studies in humans. Examination of retinal function in the intact organism (e.g., vascular or metabolic studies) provides a wealth of information, and examining the same neurons longitudinally over weeks to months, for example, to track vision loss or restoration, is also beneficial. We are relatively early in the digital imaging revolution. However, greater sensitivity, spectral range, precision, and accuracy of current approaches are expanding what may be imaged in the living eye. Moreover, on the brink of deep learning and convolutional neural network image analysis, we may be able to extract further information from increasingly rich imaging sets (Gulshan et al. 2016). New imaging abilities for exploring neurophysiological questions in humans may change the way we evaluate retinal circuits, much as noninvasive human fMRI has revolutionized the ability to image the brain. Critically, functional retinal imaging approaches will not replace, but rather complement, well-accepted existing methods such as electrophysiology. In the best of ways, multimodal approaches will provide corroborative evidence to drive conclusions when single biomarker modalities are limited. Together, they will accelerate our ability to relate the response of retinal neurons to visual perception, provide a deeper understanding of retinal physiology, diagnose retinal disease, and evaluate cutting-edge restorative/preventative therapies against retinal vision loss.

ACKNOWLEDGMENTS

We thank David Brainard for his careful and detailed review that helped us to improve our manuscript. We extend our appreciation to Jessica Morgan, Christina Schwarz, and Daniel Ts'o for very helpful insight and comments. We are very grateful to Paula Losey and Sara Peterson for assistance in manuscript and figure preparation. The authors are supported by funding from the National Eye Institute of the National Institutes of Health under awards EY028293, EY025497, EY022371, EY021166, EY004367, and P30 EY001319. Content in Figure 5c represents previously unpublished observations from a grant to Daniel Ts'o (NIH EB002843). The content is solely the responsibility of the authors and does not necessarily represent the official views of the National Institutes of Health. The authors are also supported by an Unrestricted Grant to the University of Rochester Department of Ophthalmology, a Career Development Award (J.S.) and an Ernest and Elizabeth Althouse Special Scholars Award (J.H.) from Research to Prevent Blindness, New York. J.S. is also supported by the Dana Foundation-David Mahoney Neuroimaging Grant and a research grant from Hoffman-LaRoche Inc.

DISCLOSURE STATEMENT

J.S. receives financial support from Hoffman-LaRoche, Inc. He is also an inventor on patents held by the University of Rochester. J.H. and W.M. are not aware of any affiliations, memberships, funding, or financial holdings that might be perceived as affecting the objectivity of this review.

LITERATURE CITED

Abramoff MD, Kwon YH, Ts'o D, Soliz P, Zimmerman B, et al. 2006 Visual stimulus-induced changes in human near-infrared fundus reflectance. Investig. Ophthalmol. Vis. Sci 47:715–21 [PubMed: 16431972]

Akerboom J, Carreras Calderon N, Tian L, Wabnig S, Prigge M, et al. 2013 Genetically encoded calcium indicators for multi-color neural activity imaging and combination with optogenetics. Front. Mol. Neurosci 6:2 [PubMed: 23459413]

Alm A, Bill A. 1970 Blood flow and oxygen extraction in the cat uvea at normal and high intraocular pressures. Acta Physiol. Scand 80:19–28 [PubMed: 5475327]

Ames A 3rd, Li YY, Heher EC, Kimble CR. 1992 Energy metabolism of rabbit retina as related to function: high cost of Na^+ transport. J. Neurosci 12:840–53 [PubMed: 1312136]

Asteriti S, Liu CH, Hardie RC. 2017 Calcium signalling in *Drosophila* photoreceptors measured with GCaMP6f. Cell Calcium 65:40–51 [PubMed: 28238353]

Bar-Noam AS, Farah N, Shoham S. 2016 Correction-free remotely scanned two-photon in vivo mouse retinal imaging. Light Sci. Appl 5:e16007 [PubMed: 30167112]

Beach JM, Schwenzer KJ, Srinivas S, Kim D, Tiedeman JS. 1999 Oximetry of retinal vessels by dual-wavelength imaging: calibration and influence of pigmentation. J. Appl. Physiol 86:748–58 [PubMed: 9931217]

Bedggood P, Metha A. 2012 Variability in bleach kinetics and amount of photopigment between individual foveal cones. Investig. Ophthalmol. Vis. Sci 53(7):3673–81 [PubMed: 22531694]

Blair NP, Wanek J, Felder AE, Joslin CE, Kresovich JK, et al. 2017 Retinal oximetry and vessel diameter measurements with a commercially available scanning laser ophthalmoscope in diabetic retinopathy. Investig. Ophthalmol. Vis. Sci 58:5556–63 [PubMed: 29079858]

Borghuis BG, Marvin JS, Looger LL, Demb JB. 2013 Two-photon imaging of nonlinear glutamate release dynamics at bipolar cell synapses in the mouse retina. J. Neurosci 33:10972–85 [PubMed: 23825403]

Campbell FW, Rushton WA. 1955 Measurement of the scotopic pigment in the living human eye. J. Physiol 130:131–47 [PubMed: 13278892]

Chance B, Schoener B, Oshino R, Itshak F, Nakase Y. 1979 Oxidation-reduction ratio studies of mitochondria in freeze-trapped samples. NADH and flavoprotein fluorescence signals. J. Biol. Chem 254:4764–71 [PubMed: 220260]

Chen C, Tsina E, Cornwall MC, Crouch RK, Vijayaraghavan S, Koutalos Y. 2005 Reduction of all-*trans* retinal to all-*trans* retinol in the outer segments of frog and mouse rod photoreceptors. Biophys. J 88:2278–87 [PubMed: 15626704]

Cheong SK, Strazzeri JM, Williams DR, Merigan WH. 2018 All-optical recording and stimulation of retinal neurons in vivo in retinal degeneration mice. PLOS ONE 13:e0194947 [PubMed: 29596518]

Choi KE, Yun C, Kim YH, Kim SW, Oh J, Huh K. 2017 The effect of photopigment bleaching on fundus autofluorescence in acute central serous chorioretinopathy. Retina 37:568–77 [PubMed: 27429375]

Cohen LB. 1973 Changes in neuron structure during action potential propagation and synaptic transmission. Physiol. Rev 53:373–418 [PubMed: 4349816]

Cohen LB, Salzberg BM. 1978 Optical measurement of membrane potential. Rev. Physiol. Biochem. Pharmacol 83:35–88 [PubMed: 360357]

Cooper RF, Tuten WS, Dubra A, Brainard DH, Morgan JIW. 2017 Non-invasive assessment of human cone photoreceptor function. Biomed. Opt. Express 8:5098–112 [PubMed: 29188106]

DeLint PJ, Berendschot TT, van de Kraats J, van Norren D. 2000 Slow optical changes in human photoreceptors induced by light. Investig. Ophthalmol. Vis. Sci 41:282–89 [PubMed: 10634632]

Duebel J, Haverkamp S, Schleich W, Feng G, Augustine GJ, et al. 2006 Two-photon imaging reveals somatodendritic chloride gradient in retinal ON-type bipolar cells expressing the biosensor Clomeleon. Neuron 49:81–94 [PubMed: 16387641]

Duong TQ. 2014 Magnetic resonance imaging of the retina: from mice to men. Magn. Reson. Med 71:1526–30 [PubMed: 23716429]

Duong TQ, Kim DS, Ugurbil K, Kim SG. 2002 Functional magnetic resonance imaging of the retina. Investig. Ophthalmol. Vis. Sci 43:41176

Elner SG, Elner VM, Field MG, Park S, Heckenlively JR, Petty HR. 2008 Retinal flavoprotein autofluorescence as a measure of retinal health. Trans. Am. Ophthalmol. Soc 106:215–22 [PubMed: 19277237]

Elsner AE, Burns SA, Hughes GW, Webb RH. 1992 Reflectometry with a scanning laser ophthalmoscope. Appl. Opt 31:3697–710 [PubMed: 20725343]

Erchova I, Tumlinson AR, Fergusson J, White N, Drexler W, et al. 2018 Optophysiological characterisation of inner retina responses with high-resolution optical coherence tomography. Sci. Rep 8:1813 [PubMed: 29379036]

Fan N, Silverman SM, Liu Y, Wang X, Kim BJ, et al. 2017 Rapid repeatable in vivo detection of retinal reactive oxygen species. Exp. Eye Res 161:71–81 [PubMed: 28603016]

Feke GT, Riva CE. 1978 Laser Doppler measurements of blood velocity in human retinal vessels. J. Opt. Soc. Am 68:526–31 [PubMed: 671138]

Feke GT, Zuckerman R, Green GJ, Weiter JJ. 1983 Response of human retinal blood flow to light and dark. Investig. Ophthalmol. Vis. Sci 24:136–41 [PubMed: 6826310]

Field MG, Comer GM, Kawaji T, Petty HR, Elner VM. 2012 Noninvasive imaging of mitochondrial dysfunction in dry age-related macular degeneration. Ophthalmic Surg. Lasers Imaging 43:358–65 [PubMed: 22822904]

Fox MD, Raichle ME. 2007 Spontaneous fluctuations in brain activity observed with functional magnetic resonance imaging. Nat. Rev. Neurosci 8:700–11 [PubMed: 17704812]

Frostig RD, Lieke EE, Ts'o DY, Grinvald A. 1990 Cortical functional architecture and local coupling between neuronal activity and the microcirculation revealed by in vivo high-resolution optical imaging of intrinsic signals. PNAS 87:6082–6 [PubMed: 2117272]

Garhöfer G, Bek T, Boehm AG, Gherghel D, Grunwald J, et al. 2010 Use of the retinal vessel analyzer in ocular blood flow research. Acta Ophthalmol. 88:717–22 [PubMed: 19681764]

Garhöfer G, Zawinka C, Resch H, Kothy P, Schmetterer L, Dorner GT. 2004 Reduced response of retinal vessel diameters to flicker stimulation in patients with diabetes. Br. J. Ophthalmol 88:887–91 [PubMed: 15205231]

Geirsdottir A, Palsson O, Hardarson SH, Olafsdottir OB, Kristjansdottir JV, Stefánsson E. 2012 Retinal vessel oxygen saturation in healthy individuals. Investig. Ophthalmol. Vis. Sci 53:5433–42 [PubMed: 22786895]

Grieve K, Roorda A. 2008 Intrinsic signals from human cone photoreceptors. Investig. Ophthalmol. Vis. Sci 49:713–19 [PubMed: 18235019]

Grinvald A, Lieke E, Frostig RD, Gilbert CD, Wiesel TN. 1986 Functional architecture of cortex revealed by optical imaging of intrinsic signals. Nature 324:361–64 [PubMed: 3785405]

Guevara-Torres A, Joseph A, Schallek JB. 2016 Label free measurement of retinal blood cell flux, velocity, hematocrit and capillary width in the living mouse eye. Biomed. Opt. Express 7:4228–49 [PubMed: 27867728]

Gulshan V, Peng L, Coram M, Stumpe MC, Wu D, et al. 2016 Development and validation of a deep learning algorithm for detection of diabetic retinopathy in retinal fundus photographs. JAMA 316:2402–10 [PubMed: 27898976]

Hanazono G, Tsunoda K, Kazato Y, Suzuki W, Tanifuji M. 2012 Functional topography of rod and cone photoreceptors in macaque retina determined by retinal densitometry. Investig. Ophthalmol. Vis. Sci 53:2796–803 [PubMed: 22427587]

Hanazono G, Tsunoda K, Kazato Y, Tsubota K, Tanifuji M. 2008 Evaluating neural activity of retinal ganglion cells by flash-evoked intrinsic signal imaging in macaque retina. Investig. Ophthalmol. Vis. Sci 49:4655–63 [PubMed: 18539934]

Hanazono G, Tsunoda K, Shinoda K, Tsubota K, Miyake Y, Tanifuji M. 2007 Intrinsic signal imaging in macaque retina reveals different types of flash-induced light reflectance changes of different origins. Investig. Ophthalmol. Vis. Sci 48:2903–12 [PubMed: 17525227]

Hecht S, Haig C, Chase AM. 1937 The influence of light adaptation on subsequent dark adaptation of the eye. J. Gen. Physiol 20:831–50 [PubMed: 19873031]

Heikal AA. 2010 Intracellular coenzymes as natural biomarkers for metabolic activities and mitochondrial anomalies. Biomark. Med 4:241–63 [PubMed: 20406068]

Hickam JB, Frayser R. 1966 Studies of the retinal circulation in man. Observations on vessel diameter, arteriovenous oxygen difference, and mean circulation time. Circulation 33:302–16 [PubMed: 25823104]

Hill DK, Keynes RD. 1949 Opacity changes in stimulated nerve. J. Physiol 108:278–81

Hillmann D, Spahr H, Pfäffle C, Sudkamp H, Franke G, Huttmann G. 2016 In vivo optical imaging of physiological responses to photostimulation in human photoreceptors. PNAS 113:13138–43 [PubMed: 27729536]

Hochbaum DR, Zhao Y, Farhi SL, Klapoetke N, Werley CA, et al. 2014 All-optical electrophysiology in mammalian neurons using engineered microbial rhodopsins. Nat. Methods 11:825–33 [PubMed: 24952910]

Hofer H, Carroll J, Neitz J, Neitz M, Williams DR. 2005 Organization of the human trichromatic cone mosaic. J. Neurosci 25:9669–79 [PubMed: 16237171]

Hofmann KP, Uhl R, Hoffmann W, Kreutz W. 1976 Measurements on fast light-induced light-scattering and -absorption changes in outer segments of vertebrate light sensitive rod cells. Biophys. Struct. Mech 2:61–77 [PubMed: 963228]

Huang S, Heikal AA, Webb WW. 2002 Two-photon fluorescence spectroscopy and microscopy of NAD(P)H and flavoprotein. Biophys. J 82:2811–25 [PubMed: 11964266]

Imanishi Y, Batten ML, Piston DW, Baehr W, Palczewski K. 2004 Noninvasive two-photon imaging reveals retinyl ester storage structures in the eye. J. Cell Biol 164:373–83 [PubMed: 14745001]

Izhaky D, Nelson DA, Burgansky-Eliash Z, Grinvald A. 2009 Functional imaging using the retinal function imager: direct imaging of blood velocity, achieving fluorescein angiography-like images without any contrast agent, qualitative oximetry, and functional metabolic signals. Jpn. J. Ophthalmol 53:345–51 [PubMed: 19763751]

Jia Y, Bailey ST, Hwang TS, McClintic SM, Gao SS, et al. 2015 Quantitative optical coherence tomography angiography of vascular abnormalities in the living human eye. PNAS 112:E2395–402 [PubMed: 25897021]

Keynes RD. 1951 The ionic movements during nervous activity. J. Physiol 114:119–50 [PubMed: 14861788]

Kiser PD, Golczak M, Maeda A, Palczewski K. 2012 Key enzymes of the retinoid (visual) cycle in vertebrate retina. Biochim. Biophys. Acta 1821:137–51 [PubMed: 21447403]

Klapoetke NC, Murata Y, Kim SS, Pulver SR, Birdsey-Benson A, et al. 2014 Independent optical excitation of distinct neural populations. Nat. Methods 11:338–46 [PubMed: 24509633]

Kocaoglu OP, Liu Z, Zhang F, Kurokawa K, Jonnal RS, Miller DT. 2016 Photoreceptor disc shedding in the living human eye. Biomed. Opt. Express 7:4554–68 [PubMed: 27895995]

Kornfield TE, Newman EA. 2014 Regulation of blood flow in the retinal trilaminar vascular network. J. Neurosci 34:11504–13 [PubMed: 25143628]

Lamb TD, Pugh EN Jr. 2004 Dark adaptation and the retinoid cycle of vision. Prog. Retin. Eye Res 23:307–80 [PubMed: 15177205]

Leitgeb RA, Werkmeister RM, Blatter C, Schmetterer L. 2014 Doppler optical coherence tomography. Prog. Retin. Eye Res 41:26–43 [PubMed: 24704352]

Lennie P 2003 The cost of cortical computation. Curr. Biol 13:493–97 [PubMed: 12646132]

Liem AT, Keunen JE, Van Norren D. 1996 Clinical applications of fundus reflection densitometry. Surv. Ophthalmol 41:37–50 [PubMed: 8827929]

Liem AT, Keunen JE, van Norren D, van de Kraats J. 1991 Rod densitometry in the aging human eye. Investig. Ophthalmol. Vis. Sci 32:2676–82 [PubMed: 1894467]

Ling T, Boyle KC, Goetz G, Zhou P, Quan Y, et al. 2018 Full-field interferometric imaging of propagating action potentials. Light Sci. Appl 7:107 [PubMed: 30564313]

Lu CD, Lee B, Schottenhamml J, Maier A, Pugh EN Jr., Fujimoto JG. 2017 Photoreceptor layer thickness changes during dark adaptation observed with ultrahigh-resolution optical coherence tomography. Investig. Ophthalmol. Vis. Sci 58:4632–43 [PubMed: 28898357]

Maclaurin D, Venkatachalam V, Lee H, Cohen AE. 2013 Mechanism of voltage-sensitive fluorescence in a microbial rhodopsin. PNAS 110:5939–44 [PubMed: 23530193]

Malonek D, Dirnagl U, Lindauer U, Yamada K, Kanno I, Grinvald A. 1997 Vascular imprints of neuronal activity: relationships between the dynamics of cortical blood flow, oxygenation, and volume changes following sensory stimulation. PNAS 94:14826–31 [PubMed: 9405698]

Malonek D, Grinvald A. 1996 Interactions between electrical activity and cortical microcirculation revealed by imaging spectroscopy: implications for functional brain mapping. Science 272:551–54 [PubMed: 8614805]

Martin JA, Roorda A. 2005 Direct and noninvasive assessment of parafoveal capillary leukocyte velocity. Ophthalmology 112:2219–24 [PubMed: 16257054]

Martin JA, Roorda A. 2009 Pulsatility of parafoveal capillary leukocytes. Exp. Eye Res 88:356–60 [PubMed: 18708051]

Masella BD, Hunter JJ, Williams DR. 2014 New wrinkles in retinal densitometry. Investig. Ophthalmol. Vis. Sci 55:7525–34 [PubMed: 25316726]

McGregor JE, Yin L, Yang Q, Godat T, Huynh KT, et al. 2018 Functional architecture of the foveola revealed in the living primate. PLOS ONE 13:e0207102 [PubMed: 30485298]

Michaelson IC, Friedenwald JS. 1954 Retinal Circulation in Man and Animals. Springfield, IL: Charles C Thomas

Mihashi T, Okawa Y, Miyoshi T, Kitaguchi Y, Hirohara Y, Fujikado T. 2011 Comparing retinal reflectance changes elicited by transcorneal electrical retinal stimulation with those of optic chiasma stimulation in cats. Jpn. J. Ophthalmol 55:49–56 [PubMed: 21331693]

Miura Y 2018 Two-photon microscopy (TPM) and fluorescence lifetime imaging microscopy (FLIM) of retinal pigment epithelium (RPE) of mice in vivo. Methods Mol. Biol 1753:73–88 [PubMed: 29564782]

Morgan JI, Pugh EN Jr. 2013 Scanning laser ophthalmoscope measurement of local fundus reflectance and autofluorescence changes arising from rhodopsin bleaching and regeneration. Investig. Ophthalmol. Vis. Sci 54:2048–59 [PubMed: 23412087]

Naderian A, Bussieres L, Thomas S, Lesage F, Casanova C. 2017 Cellular origin of intrinsic optical signals in the rabbit retina. Vis. Res 137:40–49 [PubMed: 28687326]

Nelson DA, Krupsky S, Pollack A, Aloni E, Belkin M, et al. 2005 Special report: noninvasive multi-parameter functional optical imaging of the eye. Ophthalmic Surg. Lasers Imaging 36:57–66 [PubMed: 15688972]

Newman EA. 2013 Functional hyperemia and mechanisms of neurovascular coupling in the retinal vasculature. J. Cereb. Blood Flow Metab 33:1685–95 [PubMed: 23963372]

Nguyen JP, Linder AN, Plummer GS, Shaevitz JW, Leifer AM. 2017 Automatically tracking neurons in a moving and deforming brain. PLOS Comput. Biol 13:e1005517 [PubMed: 28545068]

Nikonov SS, Kholodenko R, Lem J, Pugh EN Jr. 2006 Physiological features of the S- and M-cone photoreceptors of wild-type mice from single-cell recordings. J. Gen. Physiol 127:359–74 [PubMed: 16567464]

O'Connell RA, Anderson AJ, Hosking SL, Batcha AH, Bui BV. 2014 Test-retest reliability of retinal oxygen saturation measurement. Optom. Vis. Sci 91:608–14 [PubMed: 24811846]

Ogawa S, Lee TM, Kay AR, Tank DW. 1990 Brain magnetic resonance imaging with contrast dependent on blood oxygenation. PNAS 87:9868–72 [PubMed: 2124706]

Okawa Y, Fujikado T, Miyoshi T, Sawai H, Kusaka S, et al. 2007 Optical imaging to evaluate retinal activation by electrical currents using suprachoroidal-transretinal stimulation. Investig. Ophthalmol. Vis. Sci 48:4777–84 [PubMed: 17898304]

Park SJ, Kim IJ, Looger LL, Demb JB, Borghuis BG. 2014 Excitatory synaptic inputs to mouse on-off direction-selective retinal ganglion cells lack direction tuning. J. Neurosci 34:3976–81 [PubMed: 24623775]

Peng Q, Zhang Y, Nateras OS, van Osch MJ, Duong TQ. 2011 MRI of blood flow of the human retina. Magn. Reson. Med 65:1768–75 [PubMed: 21590806]

Pfäffle C, Hillmann D, Spahr H, Kutzner L, Burhan S, et al. 2018 Functional imaging of ganglion and receptor cells in living human retina by osmotic contrast. arXiv:1809.02812 [physics.bio-ph.]

Prieto PM, McLellan JS, Burns SA. 2005 Investigating the light absorption in a single pass through the photoreceptor layer by means of the lipofuscin fluorescence. Vis. Res 45:1957–65 [PubMed: 15820514]

Prunty MC, Aung MH, Hanif AM, Allen RS, Chrenek MA, et al. 2015 In vivo imaging of retinal oxidative stress using a reactive oxygen species-activated fluorescent probe. Investig. Ophthalmol. Vis. Sci 56:5862–70 [PubMed: 26348635]

Rayner CL, Gole GA, Bottle SE, Barnett NL. 2014 Dynamic, in vivo, real-time detection of retinal oxidative status in a model of elevated intraocular pressure using a novel, reversibly responsive, profluorescent nitroxide probe. Exp. Eye Res 129:48–56 [PubMed: 25447708]

Riva CE, Harino S, Shonat RD, Petrig BL. 1991 Flicker evoked increase in optic nerve head blood flow in anesthetized cats. Neurosci. Lett 128:291–96 [PubMed: 1945050]

Riva CE, Ross B, Benedek G. 1972 Laser Doppler measurements of blood flow in capillary tubes and retinal arteries. Investig. Ophthalmol. Vis. Sci 11:936–44

Roorda A, Williams DR. 1999 The arrangement of the three cone classes in the living human eye. Nature 397:520–22 [PubMed: 10028967]

Roy CS, Sherrington CS. 1890 On the regulation of the blood-supply of the brain. J. Physiol 11:85–158.17

Rushton WA. 1956 The difference spectrum and the photosensitivity of rhodopsin in the living human eye. J. Physiol 134:11–29 [PubMed: 13377309]

Sabesan R, Hofer H, Roorda A. 2015 Characterizing the human cone photoreceptor mosaic via dynamic photopigment densitometry. PLOS ONE 10:e0144891 [PubMed: 26660894]

Sabesan R, Schmidt BP, Tuten WS, Roorda A. 2016 The elementary representation of spatial and color vision in the human retina. Sci. Adv 2:e1600797 [PubMed: 27652339]

Schallek JB, Geng Y, Nguyen H, Williams DR. 2013 Morphology and topography of retinal pericytes in the living mouse retina using in vivo adaptive optics imaging and ex vivo characterization. Investig. Ophthalmol. Vis. Sci 54:8237–50 [PubMed: 24150762]

Schallek JB, Kardon R, Kwon Y, Abramoff M, Soliz P, Ts'o D. 2009a Stimulus-evoked intrinsic optical signals in the retina: Pharmacologic dissection reveals outer retinal origins. Investig. Ophthalmol. Vis. Sci 50:4873–80 [PubMed: 19420331]

Schallek JB, Li H, Kardon R, Kwon Y, Abramoff M, et al. 2009b Stimulus-evoked intrinsic optical signals in the retina: spatial and temporal characteristics. Investig. Ophthalmol. Vis. Sci 50:4865–72 [PubMed: 19420337]

Schallek JB, McLellan GJ, Viswanathan S, Ts'o DY. 2012 Retinal intrinsic optical signals in a cat model of primary congenital glaucoma. Investig. Ophthalmol. Vis. Sci 53:1971–81 [PubMed: 22395886]

Schallek JB, Ts'o D. 2011 Blood contrast agents enhance intrinsic signals in the retina: evidence for an underlying blood volume component. Investig. Ophthalmol. Vis. Sci 52:1325–35 [PubMed: 21051719]

Schwarz C, Sharma R, Cheong SK, Keller M, Williams DR, Hunter JJ. 2018 Selective S cone damage and retinal remodeling following intense ultrashort pulse laser exposures in the near-infrared. Investig. Ophthalmol. Vis. Sci 59:5973–84 [PubMed: 30556839]

Schwarz C, Sharma R, Fischer WS, Chung M, Palczewska G, et al. 2016 Safety assessment in macaques of light exposures for functional two-photon ophthalmoscopy in humans. Biomed. Opt. Express 7:5148–69 [PubMed: 28018732]

Schweitzer D, Hammer M, Kraft J, Thamm E, Konigsdorffer E, Strobel J. 1999 In vivo measurement of the oxygen saturation of retinal vessels in healthy volunteers. IEEE Trans. Biomed. Eng 46:1454–65 [PubMed: 10612903]

Sharma R, Schwarz C, Hunter JJ, Palczewska G, Palczewski K, Williams DR. 2017 Formation and clearance of all-*trans*-retinol in rods investigated in the living primate eye with two-photon ophthalmoscopy. Investig. Ophthalmol. Vis. Sci 58:604–13 [PubMed: 28129424]

Sharma R, Schwarz C, Williams DR, Palczewska G, Palczewski K, Hunter JJ. 2016a In vivo two-photon fluorescence kinetics of primate rods and cones. Investig. Ophthalmol. Vis. Sci 57:647–57 [PubMed: 26903225]

Sharma R, Williams DR, Palczewska G, Palczewski K, Hunter JJ. 2016b Two-photon autofluorescence imaging reveals cellular structures throughout the retina of the living primate eye. Investig. Ophthalmol. Vis. Sci 57:632–46 [PubMed: 26903224]

Shmuel A, Yacoub E, Pfeuffer J, Van de Moortele PF, Adriany G, et al. 2002 Sustained negative BOLD, blood flow and oxygen consumption response and its coupling to the positive response in the human brain. Neuron 36:1195–210 [PubMed: 12495632]

Singh AS, Kolbitsch C, Schmoll T, Leitgeb RA. 2010 Stable absolute flow estimation with Doppler OCT based on virtual circumpapillary scans. Biomed. Opt. Express 1:1047–58 [PubMed: 21258529]

Stefánsson E, Olafsdottir OB, Einarsdottir AB, Eliasdottir TS, Eysteinsson T, et al. 2017 Retinal oximetry discovers novel biomarkers in retinal and brain diseases. Investig. Ophthalmol. Vis. Sci 58:BIO27–33 [PubMed: 28475700]

Stepanenko OV, Verkhusha VV, Kuznetsova IM, Uversky VN, Turoverov KK. 2008 Fluorescent proteins as biomarkers and biosensors: throwing color lights on molecular and cellular processes. Curr. Protein Pept. Sci 9:338–69 [PubMed: 18691124]

Stockman A, Sharpe LT. 2000 The spectral sensitivities of the middle- and long-wavelength-sensitive cones derived from measurements in observers of known genotype. Vis. Res 40:1711–37 [PubMed: 10814758]

Stokes GG. 1863 On the reduction and oxidation of the colouring matter of the blood. Proc. R. Soc. Lond 13:355–64

Suzuki W, Tsunoda K, Hanazono G, Tanifuji M. 2013 Stimulus-induced changes of reflectivity detected by optical coherence tomography in macaque retina. Investig. Ophthalmol. Vis. Sci 54:6345–54 [PubMed: 23982841]

Tam J, Roorda A. 2011 Speed quantification and tracking of moving objects in adaptive optics scanning laser ophthalmoscopy. J. Biomed. Opt 16:036002 [PubMed: 21456866]

Thapa D, Wang B, Lu Y, Son T, Yao X. 2017 Enhancement of intrinsic optical signal recording with split spectrum optical coherence tomography. J. Mod. Opt 64:1800–7 [PubMed: 29129961]

Theelen T, Berendschot TT, Boon CJ, Hoyng CB, Klevering BJ. 2008 Analysis of visual pigment by fundus autofluorescence. Exp. Eye Res 86:296–304 [PubMed: 18096158]

Thestrup T, Litzlbauer J, Bartholomaus I, Mues M, Russo L, et al. 2014 Optimized ratiometric calcium sensors for functional in vivo imaging of neurons and T lymphocytes. Nat. Methods 11:175–82 [PubMed: 24390440]

Ts'o DY, Frostig RD, Lieke EE, Grinvald A. 1990 Functional organization of primate visual cortex revealed by high resolution optical imaging. Science 249:417–20 [PubMed: 2165630]

Ts'o DY, Schallek J, Kwon Y, Kardon R, Abramoff M, Soliz P. 2009 Noninvasive functional imaging of the retina reveals outer retinal and hemodynamic intrinsic optical signal origins. Jpn. J. Ophthalmol 53:334–44 [PubMed: 19763750]

Tsunoda K, Oguchi Y, Hanazono G, Tanifuji M. 2004 Mapping cone- and rod-induced retinal responsiveness in macaque retina by optical imaging. Investig. Ophthalmol. Vis. Sci 45:3820–26 [PubMed: 15452094]

Uddin MI, Evans SM, Craft JR, Capozzi ME, McCollum GW, et al. 2016 In vivo imaging of retinal hypoxia in a model of oxygen-induced retinopathy. Sci. Rep 6:31011 [PubMed: 27491345]

Uddin MI, Jayagopal A, McCollum GW, Yang R, Penn JS. 2017 In vivo imaging of retinal hypoxia using HYPOX-4-dependent fluorescence in a mouse model of laser-induced retinal vein occlusion (RVO). Investig. Ophthalmol. Vis. Sci 58:3818–24

van de Kraats J, Berendschot TT, van Norren D. 1996 The pathways of light measured in fundus reflectometry. Vis. Res 36:2229–47 [PubMed: 8776488]

van Norren D, van de Kraats J. 1989 Imaging retinal densitometry with a confocal scanning laser ophthalmoscope. Vis. Res 29:1825–30 [PubMed: 2631402]

Vanzetta I, Deneux T, Grinvald A. 2014 High-resolution wide-field optical imaging of microvascular characteristics: from the neocortex to the eye In Neurovascular Coupling Methods, ed. Zhao M, Ma H, Schwartz TH, pp. 123–59. New York: Humana Press

Vo Van Toi Riva CE. 1995 Variations of blood flow at optic nerve head induced by sinusoidal flicker stimulation in cats. J. Physiol 482 (Pt. 1):189–202. Erratum. 1995. J. Physiol. 484 (Pt. 3):811 [PubMed: 7730982]

Wall NR, Wickersham IR, Cetin A, De La Parra M, Callaway EM. 2010 Monosynaptic circuit tracing in vivo through Cre-dependent targeting and complementation of modified rabies virus. PNAS 107:21848–53 [PubMed: 21115815]

Walters S, Schwarz C, Sharma R, Rossi EA, Fischer W, et al. 2019 Cellular-scale evaluation of induced photoreceptor degeneration in the living primate eye. Biomed. Opt. Express 10:66–82 [PubMed: 30775083]

Wang B, Lu Y, Yao X. 2016 In vivo optical coherence tomography of stimulus-evoked intrinsic optical signals in mouse retinas. J. Biomed. Opt 21:96010 [PubMed: 27653936]

Wang JS, Kefalov VJ. 2011 The cone-specific visual cycle. Prog. Retin. Eye Res 30:115–28 [PubMed: 21111842]

Wang TM, Holzhausen LC, Kramer RH. 2014 Imaging an optogenetic pH sensor reveals that protons mediate lateral inhibition in the retina. Nat. Neurosci 17:262–68 [PubMed: 24441679]

Wells-Gray EM, Choi SS, Zawadzki RJ, Finn SC, Greiner C, et al. 2018 Volumetric imaging of rod and cone photoreceptor structure with a combined adaptive optics-optical coherence tomography-scanning laser ophthalmoscope. J. Biomed. Opt 23:1–15

Wong-Riley MT. 2010 Energy metabolism of the visual system. Eye Brain 2:99–116 [PubMed: 23226947]

Xu Y, Zou P, Cohen AE. 2017 Voltage imaging with genetically encoded indicators. Curr. Opin. Chem. Biol 39:1–10 [PubMed: 28460291]

Yang HH, St-Pierre F, Sun X, Ding X, Lin MZ, Clandinin TR. 2016 Subcellular imaging of voltage and calcium signals reveals neural processing in vivo. Cell 166:245–57 [PubMed: 27264607]

Yao X, Wang B. 2015 Intrinsic optical signal imaging of retinal physiology: a review. J. Biomed. Opt 20:090901 [PubMed: 26405819]

Yellen G, Mongeon R. 2015 Quantitative two-photon imaging of fluorescent biosensors. Curr. Opin. Chem. Biol 27:24–30 [PubMed: 26079046]

Yin L, Geng Y, Osakada F, Sharma R, Cetin AH, et al. 2013 Imaging light responses of retinal ganglion cells in the living mouse eye. J. Neurophysiol 109:2415–21 [PubMed: 23407356]

Yin L, Masella B, Dalkara D, Zhang J, Flannery JG, et al. 2014 Imaging light responses of foveal ganglion cells in the living macaque eye. J. Neurosci 34:6596–605 [PubMed: 24806684]

Yu DY, Cringle SJ. 2001 Oxygen distribution and consumption within the retina in vascularised and avascular retinas and in animal models of retinal disease. Prog. Retin. Eye Res 20:175–208 [PubMed: 11173251]

Yuan S, Roney CA, Wierwille J, Chen CW, Xu B, et al. 2010 Co-registered optical coherence tomography and fluorescence molecular imaging for simultaneous morphological and molecular imaging. Phys. Med. Biol 55:191–206 [PubMed: 20009192]

Zhang LL, Pathak HR, Coulter DA, Freed MA, Vardi N. 2006 Shift of intracellular chloride concentration in ganglion and amacrine cells of developing mouse retina. J. Neurophysiol 95:2404–16 [PubMed: 16371454]

Zhang P, Zawadzki RJ, Goswami M, Nguyen PT, Yarov-Yarovoy V, et al. 2017 In vivo optophysiology reveals that G-protein activation triggers osmotic swelling and increased light scattering of rod photoreceptors. PNAS 114:E2937–46 [PubMed: 28320964]

Zhang Q, Lu R, Wang B, Messinger JD, Curcio CA, Yao X. 2015 Functional optical coherence tomography enables in vivo physiological assessment of retinal rod and cone photoreceptors. Sci. Rep 5:9595 [PubMed: 25901915]

Zhang QX, Lu RW, Li YG, Yao XC. 2011 In vivo confocal imaging of fast intrinsic optical signals correlated with frog retinal activation. Opt. Lett 36:4692–94 [PubMed: 22139286]

Zhong Z, Huang G, Chui TY, Petrig BL, Burns SA. 2012 Local flicker stimulation evokes local retinal blood velocity changes. J. Vis 12:3

OVERVIEW OF RETINAL STRUCTURE

A photoreceptor is comprised of an outer segment with folds of membrane densely packed with photopigment, an inner segment densely packed with mitochondria, a soma, and a proximal synaptic terminal. Long, narrow, and cylindrically shaped rods dominate the peripheral retina and are primarily responsible for low-light vision (scotopic). Cones are responsible for vision at high light levels (photopic), color vision, and high spatial acuity vision in the center of the visual field at the fovea where they are densely packed. At greater eccentricities, cones are larger and less densely packed. There are three types of cones, classified by their short-, medium-, and long-wavelength sensitivities. Through phototransduction, photon absorption by the photoreceptors is transmitted to the horizontal (involved in lateral inhibition) and bipolar cells. The latter begin the process of integrating and comparing signals as they relay information to the dendritic arbors of ganglion cells. These dendritic fields connect with both ganglion and amacrine cells in the inner plexiform layer. Ganglion cells further process these signals before relaying information to the brain through their axons, which form the nerve fiber layer, leave the retina through the optic nerve head, and terminate at the lateral geniculate nucleus and other midbrain structures. Many excellent resources including the Webvision website (https://webvision.med.utah.edu/) provide additional details.

Holangiotic retina:

retina with vessel plexus in the neural retina, including primates, carnivores, and most rodents, but not rabbits, horses, and birds

SUMMARY POINTS

1. Photoreceptor responses to light have been measured by a variety of noninvasive imaging techniques, revealing modulations of backscattered light and changes in optical path length of outer segments in response to light.
2. Near-infrared intrinsic signal imaging of the retina has shown positive and negative reflectance changes that are not impacted by photopigment changes.
3. Many imaging modalities have examined vascular light responses and neurovascular coupling in the retina, measuring retinal vessel caliber, flow, and oxygenation.
4. Imaging of autofluorescent compounds native to the retina is a new direction toward noninvasive imaging that may reveal the modulation of both metabolic processes and aspects of the visual cycle within cells of the living eye.
5. Imaging extrinsic fluorophores can boost the contrast of specific physiological processes in retinal neurons. For example, responses of ganglion cells have been studied using calcium indicators of neuronal function.
6. Imaging of functional responses of the inner retina is often overshadowed by stronger outer retinal responses.
7. Collective advantages of these in vivo imaging techniques include the tracking of visual response over time, greater understanding of normal physiology, surveillance of disease, and increased testing efficacy of vision restoration.

FUTURE ISSUES

1. Combining multiple modalities will be essential to understand and take advantage of the complex interplay of the myriad of biological reporters. For example, optical coherence tomography combined with adaptive optics two-photon excited fluorescence imaging would be far more informative than the same methods used separately.
2. Work remains to make the imaging tools discussed here more widely accessible and adopted by investigators. These goals involve both the commercialization of new instrumentation and the demonstration of its research and clinical value.
3. Toward these goals, there needs to be continued improvement of both instrumentation (e.g., detectors, new modalities) and biological reporters (e.g., indicators for voltage, neurotransmitters, ions, metabolic function such as glucose and NADH).
4. Limitations of in vivo imaging include the difficulty of studying the majority of postreceptoral cells in the retina and the need to optimize reporters for inner retinal function. Owing to new advances in phase-contrast techniques, these cells can now be visualized and tracked, which provides an exciting step forward to measuring their function.

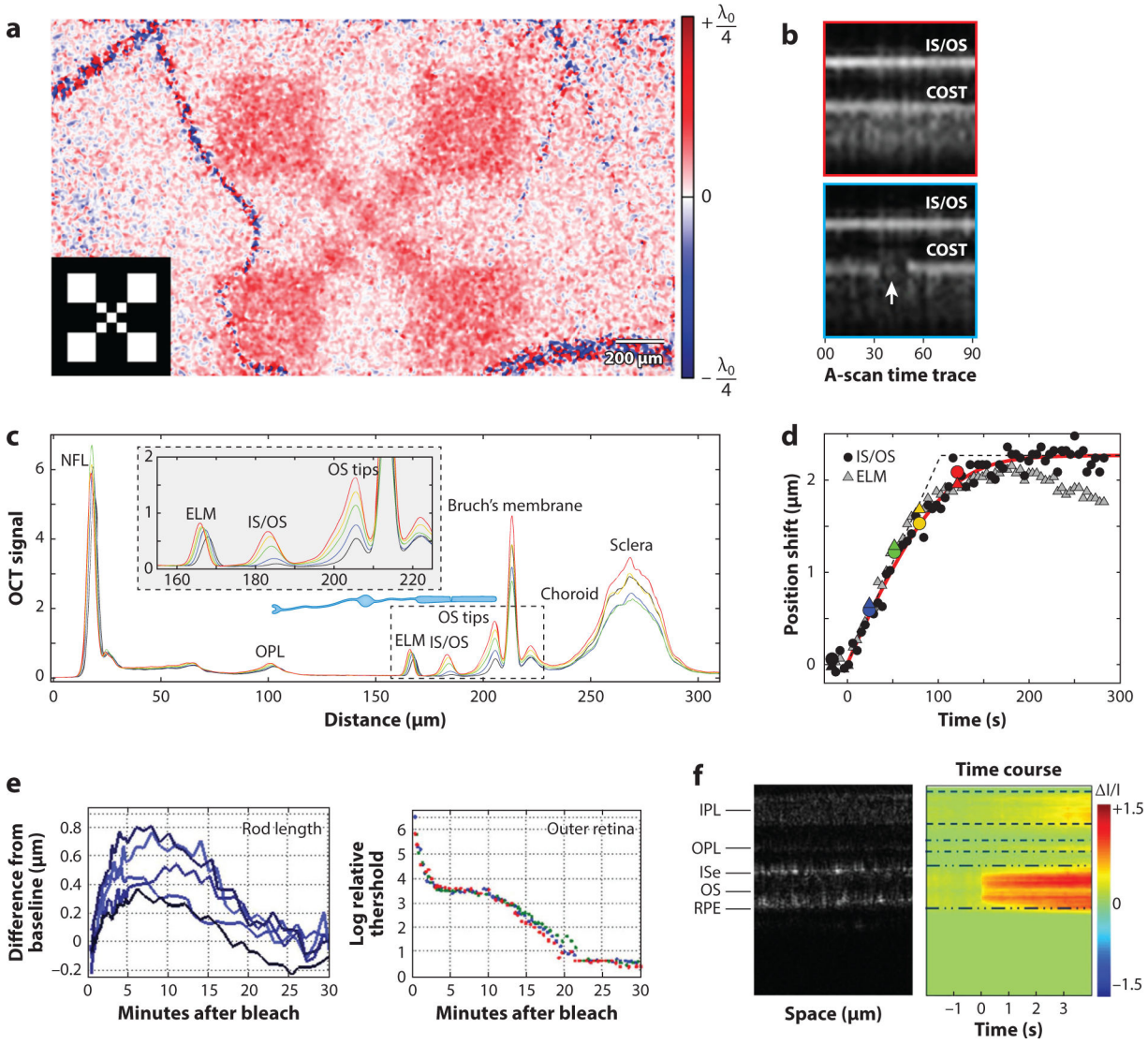

Figure 1.

OCT functional responses. (*a*) Spatial pattern of optical path length of human photoreceptors measured with OCT in response to pattern stimulus (*lower left corner*) (Hillmann et al. 2016). (*b*) OCT A-scan time trace of two representative human cones (*red* and *blue*) over 90 min. The location of IS/OS border and COST are shown. The COST of the lower cone disappears from minute 33 to minute 51 (*white arrow*) and then reappears displaced toward the IS/OS junction. Panel *b* adapted with permission Kocaoglu et al. (2016); copyright 2016, The Optical Society. (*c*) Profile of OCT signal across mouse outer retina measured before (*black*) and 25 s (*blue*), 52 s (*green*), 80 s (*yellow*), and 121 s (*red*) after a brief stimulus: (*detail inset*) magnification of outer retinal profile. The distance from Bruch's membrane to NFL does not change. However, the positions of other retinal layers, most notably the ELM, IS/OS junction, and OS tips are shifted toward the inner retina, indicating elongation of the IS and OS of the photoreceptors (Zhang et al. 2017). (*d*) This elongation is plotted over time for the distance from ELM and IS/OS to Bruch's membrane (Zhang et al. 2017). (*e*) Length of human rods and dark adaptation sensitivity more than 30 min following a bright flash of

blue light bleaching 96% of rhodopsin. The recovery of rod length after ~10 min is correlated with the recovery of visual sensitivity during dark adaptation (Lu et al. 2017). (*f*) A single OCT B-scan image of mouse photoreceptors is shown for orientation (*left*) beside a differential plot showing intensity profile over time in response to stimulation (*right*); outer retinal activation (OS) precedes a weaker response of postreceptoral inner plexiform layer (IPL). Panel *f* adapted with permission from Thapa et al. (2017); copyright 2017, Taylor & Francis, Ltd. Abbreviations: COST, cone outer segment tip; ELM, external limiting membrane; IPL, inner plexiform layer; IS, inner segment; ISe, inner segment ellipsoid; NFL, nerve fiber layer; OCT, optical coherence tomography; OPL, outer plexiform layer; OS, outer segment; RPE, retinal pigment epithelium.

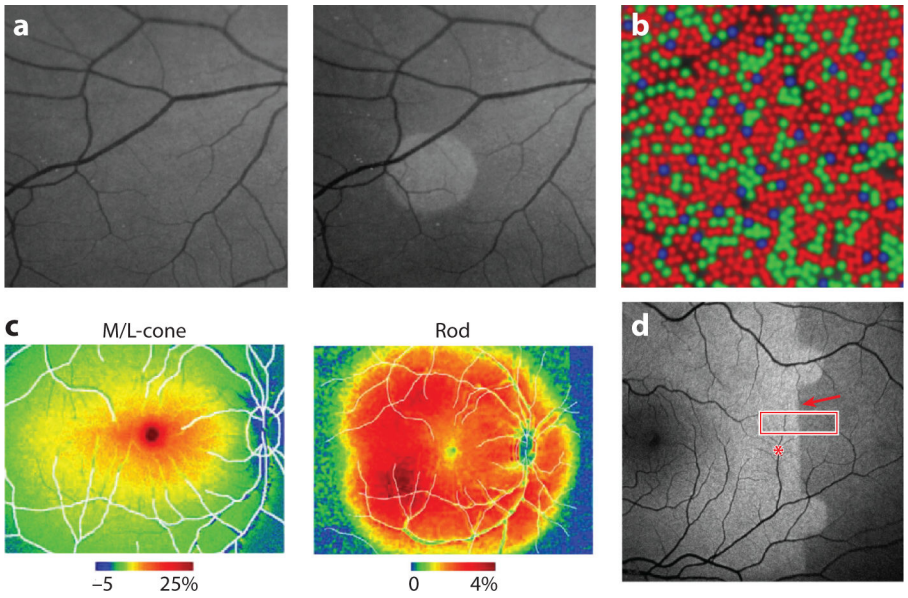

Figure 2.

Photopigment densitometry. (*a*) Scanning laser ophthalmoscope images in human show a localized increase in reflectance in response to a focal 4.8° circular stimulus (532 nm, 1.5×10^7 scot Td-s) (*right*) Stimulus response compared with the dark-adapted state is evident with the naked eye (*left*). Panel *a* adapted from adapted with permission from Morgan & Pugh (2013). (*b*) Selective cone bleaching with an adaptive optics scanning light ophthalmoscope allows classification of individual human cones. S (*blue*), M (*green*), and L (*red*) are shown in false colors overlaid on an image of the cone mosaic (Sabesan et al. 2015). Scale bar: 2 arcmin. (*c*) Photopigment distribution maps of M/L cones (*left*) and rods (*right*) are consistent with expected cell topography in macaque. The color map represents the reflectance change following illumination with 5.35 log phot Td between 60 s and 180 s for M/L cones and with 4.73 log scot Td between 52.5 s and 150 s for rods. Panel *b* adapted with permission from Hanazono et al. (2012). Horizontal dimensions are ~35° and ~60° for M/L cone and rod images, respectively. (*d*) Exposure of human retina to 488 nm excitation light in a scanning light ophthalmoscope (Heidelberg Retina Angiograph 2, Heidelberg Engineering) leads to an increase in emitted fluorescence >520 nm with a border matching the shape of a mirror within the instrument. The increased fluorescence may indicate that photopigment bleaching reduces photoreceptor screening of lipofuscin fluorescence. Panel *d* adapted with permission Theelen et al. (2008); copyright 2008, The Optical Society.

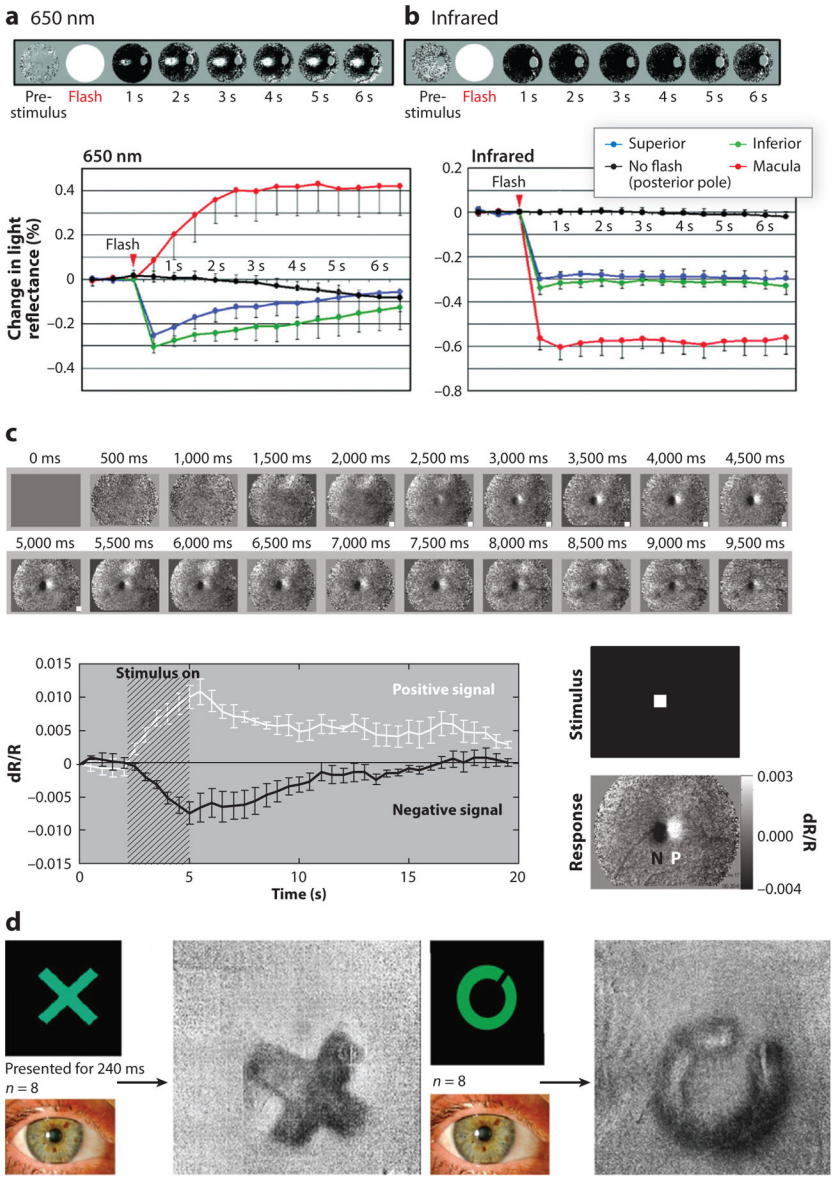

Figure 3.

Near-infrared intrinsic signals in macaque, cat, and human. (*a*) In macaque, visible light reflectance increases in the macula and decreases in the periphery in response to a short flash of white light (consistent with conventional densitometry): (*top*) visualized and (*bottom*) quantified time progressions. (*b*) Using the same preparation, imaging with near-infrared light shows a global decrease in reflectance across the retina. Panels *a* and *b* adapted with permission from Tsunoda et al. (2004). (*c*) In cat, focal stimulation with a small spot of visible light reveals activations of a negative- and positive-evoked response: (*white squares*) time when stimulus was present. There is a slow, continuous rise of signal during stimulus and a slow recovery of each signal back to baseline. Panel *c* adapted with permission Ts'o et al. (2009); copyright 2009, Japanese Ophthalmology Society. (*d*) In human, focal retinal response to patterned stimuli in a commercial device shows spatially precise activations.

Panel *d* adapted from with permission from Vanzetta et al. (2014); copyright 2014, Springer Nature. Abbreviation: dR/R, change in reflectance normalized by baseline reflectance.

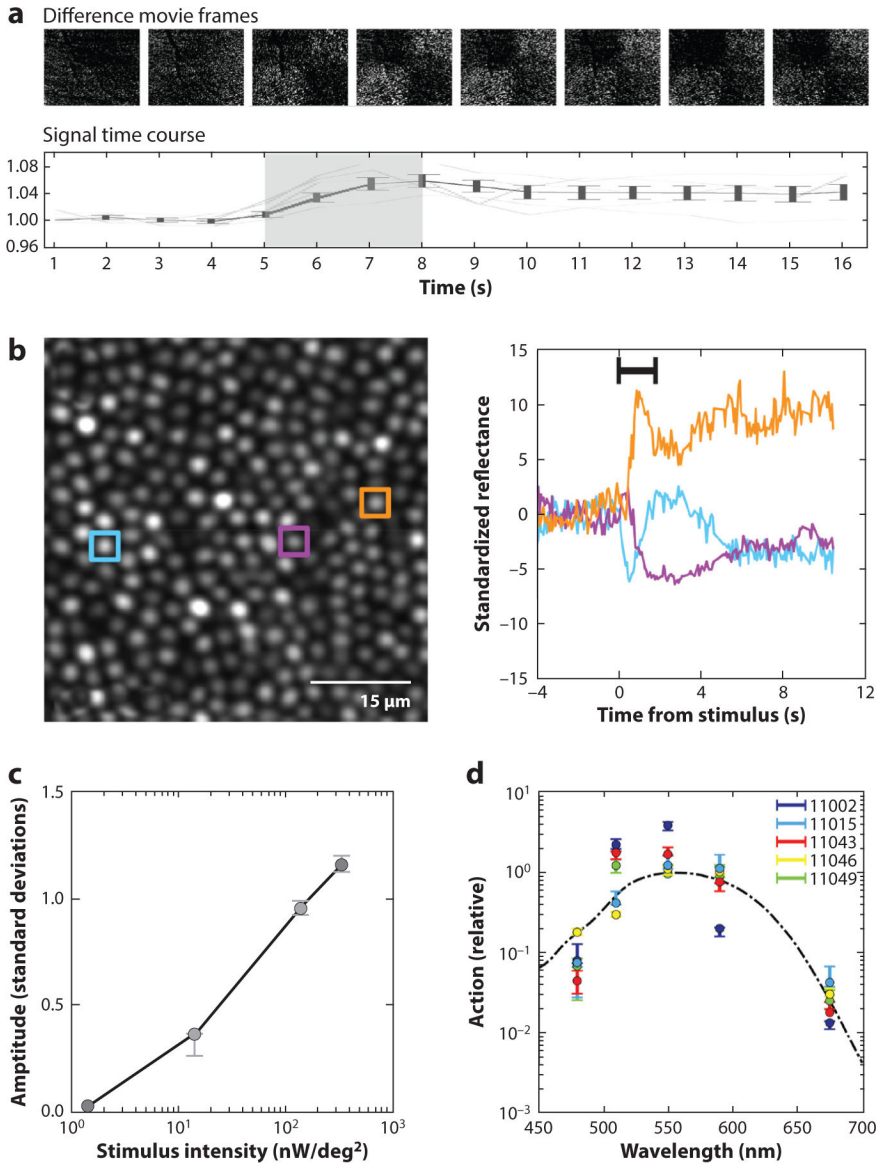

Figure 4.

Photoreceptor imaging using adaptive optics scanning light ophthalmoscope reveals single-cell changes in response to light. (*a*) Human retina shows spatially precise activations in response to a 2 × 2 checkerboard pattern. Net response is an increase in normalized 840-nm backscatter that grows during 658-nm stimulus presentation. Panel *a* adapted with permission from Grieve & Roorda (2008). (*b*) Single photoreceptors show variable responses to light presentation in the human retina. Some cones increase in reflectance, whereas others decrease. Cells often show a unique temporal response profile. (*c*) Photoreceptor response determined by measuring signal variance relative to baseline, as the evoked response grows in amplitude in correspondence with brighter visual stimuli. (*d*) Photoreceptor responses matched the human photopic luminosity function in five human subjects when tested with stimuli at different visible wavelengths. Panels *b*–*d* adapted with permission from Cooper et al. (2017); copyright 2017, The Optical Society.

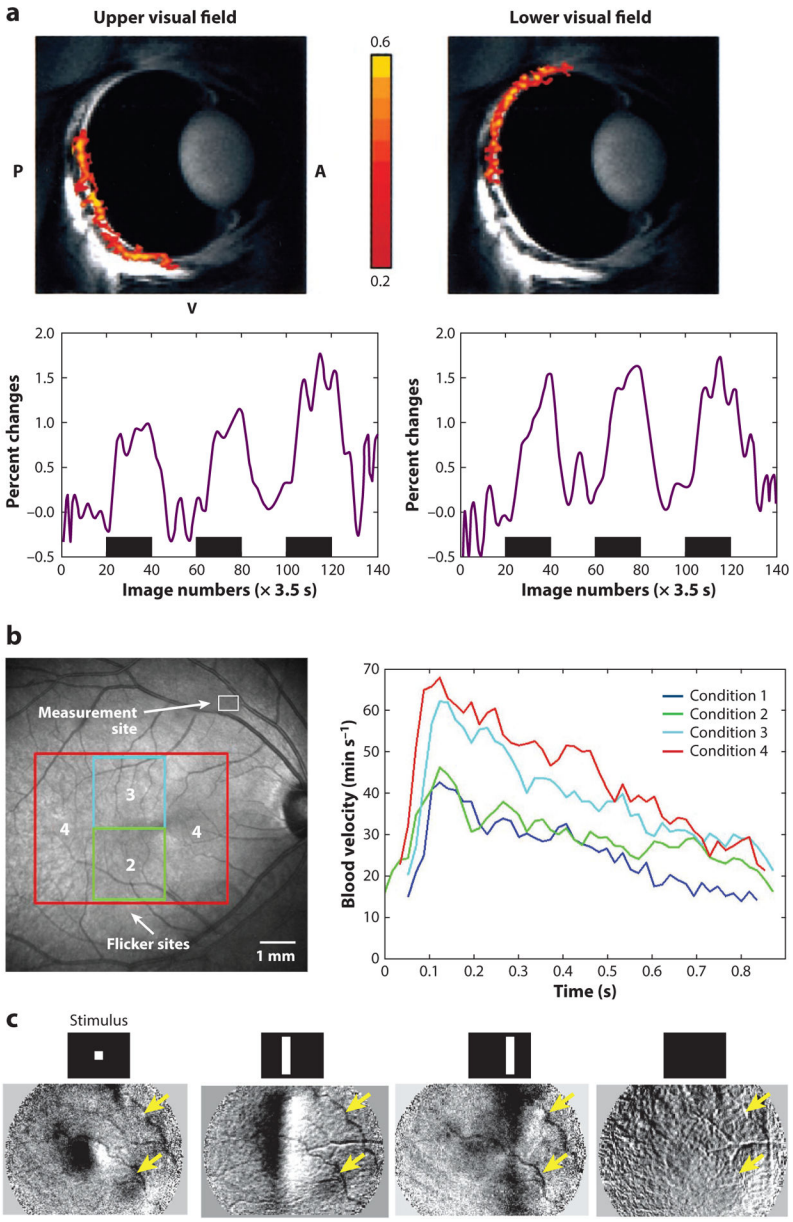

Figure 5.

Imaging the neurovascular response to visual stimulation. (*a*) Functional magnetic resonance imaging reveals focal activations of cat retina. Inferior and superior retina show independent activations with blood-oxygen-level-dependent signals in response to visual stimulation. Panel *a* adapted with permission from Duong et al. (2002). (*b*) Blood velocity of a single arteriole (measurement site) is tracked using an adaptive optics scanning-light ophthalmoscope in response to four different flicker sites. Blood velocity modulation reflects two aspects. First, all plots show the cardiac pulse wave. Second, only stimuli that fall within the watershed area of the imaged arteriole show velocity modulations in response to flicker (*conditions 3* and *4*). Condition 1 (no stimulus) and condition 2 (presumably supplied from other vessels) do not show a differential response. Panel *b* adapted with permission from Zhong et al. (2012) (*c*) In cat, near-infrared reflectance imaging of focal

activations shows vessel darkening far from stimulus sites, indicating putative increase in blood volume. Active vessels do not appear in response to blank condition (*far right*) (J.B. Schallek, unpublished observations). Abbreviations: A, anterior; P, posterior; V, ventral.

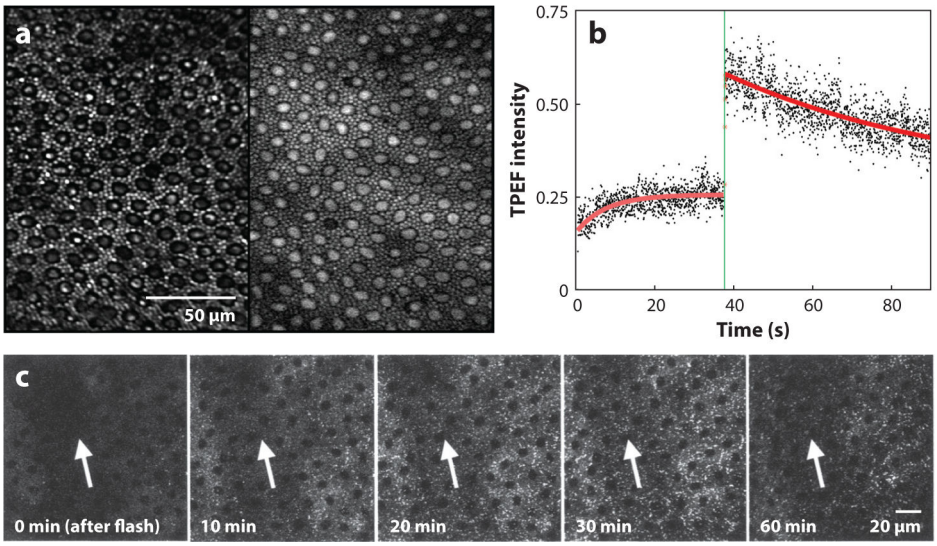

Figure 6.

Two-photon excited fluorescence (TPEF) imaging of intrinsic visual cycle fluorophores. (*a*) Individual macaque rods and cones visualized with infrared reflectance (*left*) and TPEF (*right*) adaptive optics scanning light ophthalmoscope. (*b*) Fluorescence from macaque rod locations increases exponentially in response to 730 nm light used for TPEF imaging. An additional brief flash of 561 nm light (7.35 log scotopic Td-s for 0.175 s) (*vertical green line*) bleaches 98% of photopigment and leads to a rapid increase and subsequent exponential decease in emitted TPEF likely corresponding to rapid production and clearance of all-*trans*-retinol from rods (Sharma et al. 2017). (*c*) TPEF images of retinosomes (*bright spots*) in mouse retinal pigment epithelium at multiple time points after flash stimulation. The fluorescence increases approximately three times in the 20–30 min post-stimulation (Imanishi et al. 2004). The brightness of images has been adjusted 10% for reproduction.

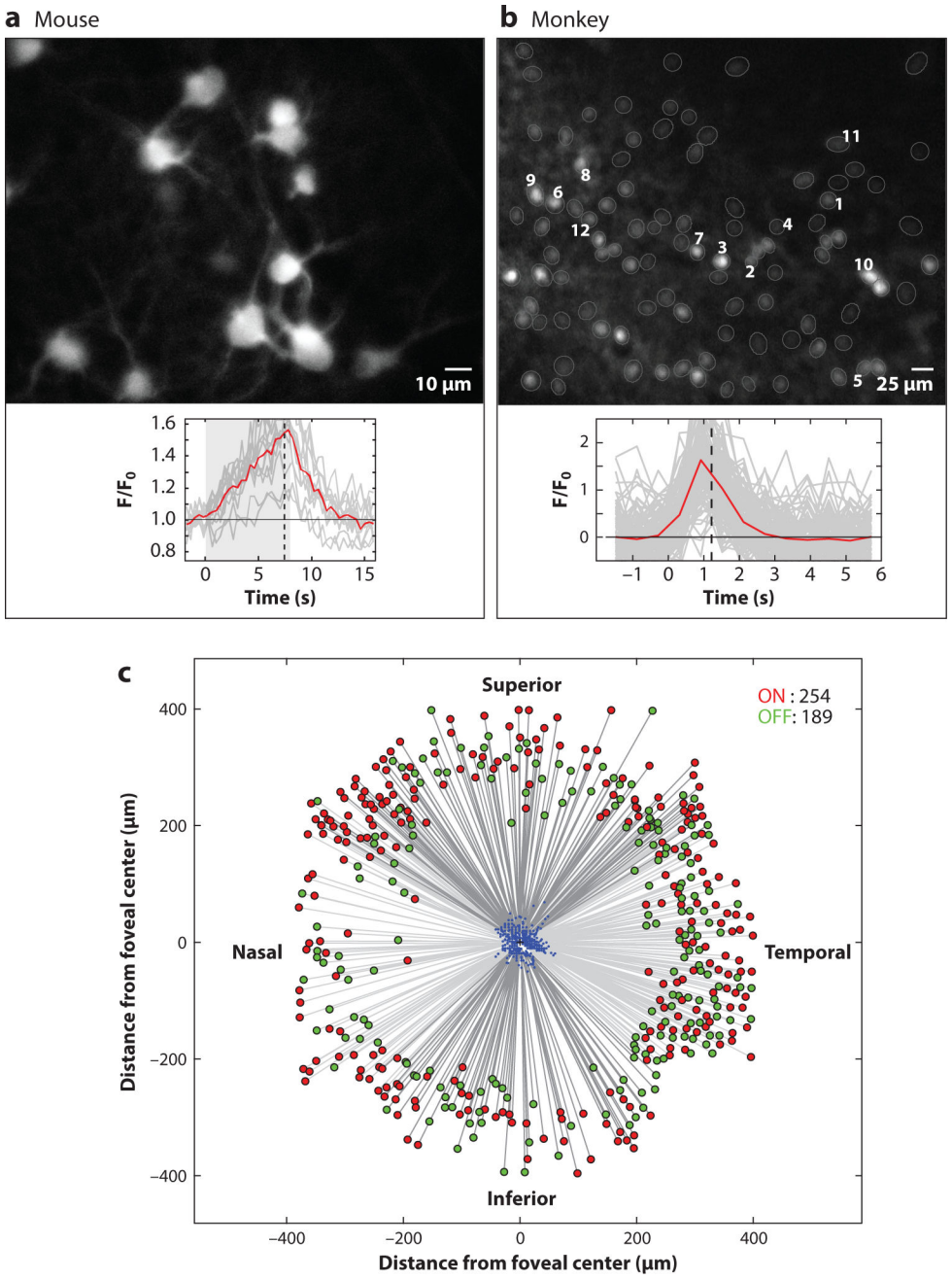

Figure 7.

Fluorescent calcium responses of ganglion cells in mouse and macaque retina. (*a*) GCaMP3 is expressed in mouse ganglion cells (*upper panel*). Tracking fluorescence in a single cell shows repeatable activations in response to presentations of an 8-s ultraviolet stimulus. Panel *a* adapted with permission from Yin et al. (2013); copyright 2013, American Physiological Society. (*b*) GCaMP5 is expressed in macaque ganglion cells surrounding the fovea (*upper panel*). The lower plot shows the fluorescence response to a 1-s visible stimulus presented at time 0. Panel *b* adapted with permission from Yin et al. (2014); copyright 2014, Society for Neuroscience. (*c*) In monkey, microscopic stimuli (*blue dots*) were presented at the foveola

to measure the receptive field of displaced ganglion cells labeled with GCaMP6. Both ON (*red*) and OFF (*green*) cells show a consistent displacement radiating from the fovea center (McGregor et al. 2018).